Clumped isotope thermometry in foraminifera as a tool in paleoceanography: New planktic and benthic data and constraints on non-thermal effects

Aradhna Tripati[1,2*], Hannah Tandy[1*], Alexandra Villa[1,3*], Randon J. Flores[1], Alexandrea Arnold[2], Hannah Carroll[1], Maxence Guillermic[1,2], Ingrid Maradiaga[2], Cristian Blair[2], Bisrat Zerehaimanot[2], Dana Brown[2], Robert Ulrich[1,2], Cristian-Roman Palacios[2], Julia de La Cruz[1], Mohan Kuppusamy[4], Dharmendra Pratap Singh[5], Raquel Bryant[6], Fengming Chang[7], Robert A. Eagle[2], Ceara Tomaiso[8], Thomas M. Marchitto[9], Rosemarie E. Came[8], Jean Lynch-Stieglitz[10]

[1]Department of Earth Planetary and Space Sciences, University of California, Los Angeles, 595 Charles Young Dr East, Los Angeles, California 90095 USA.

[2]Department of Atmospheric and Oceanic Sciences, Institute of the Environment and Sustainability, Center for Diverse Leadership in Science, American Indian Studies Center, University of California, Los Angeles, California, Los Angeles, USA.

[3]Department of Geoscience, University of Wisconsin - Madison. Lewis G. Weeks Hall, 1215 W Dayton St, Madison, WI 53706 USA.

[4]School of Civil Engineering, Vellore Institute of Technology, Chennai 600127, India

[5]Department of Earth Sciences, Indian Institute of Technology Roorkee, Roorkee, Uttarakhand-247667, India

[6]Department of Earth and Environmental Sciences, Wesleyan University, 265 Church St. Middletown, CT 06459 USA.

[7]Key Laboratory of Marine Geology and Environment, Institute of Oceanology, Chinese Academy of Sciences, Qingdao 266071, China

[8]Earth Sciences Department, University of New Hampshire, James Hall Rm 214, Durham, NH 03824 USA.

[9]Department of Geological Sciences, University of Colorado Boulder, Boulder, CO, USA

[10]School of Earth and Atmospheric Sciences, Georgia Institute of Technology, Atlanta, GA, USA

Corresponding authors: Aradhna Tripati (atripati@g.ucla.edu), Hannah Tandy (htandy1234@g.ucla.edu), Alexandra Villa (avilla2@wisc.edu)

Key Points:

- We report a foraminiferal temperature calibration: $\Delta_{47} = 0.0374 \pm 0.0013\ 10^6/T^2 + 0.1744 \pm 0.0154$; n = 260; >2500 analyses).
- A multivariate regression for benthics is $\Delta_{47} = 0.152 \pm 0.049 + 0.03865 \pm 0.00376 \times 10^6/T^2 + 0.000150 \pm 0.0000601\ \Delta[CO_3^{2-}]$ (n = 42)
- We apply the regressions to published Cenozoic data and show they yield more reasonable temperature and seawater $\delta^{18}O$ estimates.

Abstract

The carbonate "clumped" isotope thermometer (Δ_{47}) in foraminifera is increasingly being used to reconstruct ocean temperature. Here we address several less understood aspects of the proxy using a large dataset comprising new and reprocessed data. The Δ_{47}-temperature relationship in foraminifera (n = 260) is described by $\Delta_{47} = 0.0374 \pm 0.0013\ 10^6/T^2 + 0.1744 \pm 0.0154$, and in inorganic calcite (n = 118) by $\Delta_{47} = 0.0392 \pm 0.0014\ 10^6/T^2 + 0.1547 \pm 0.0165$. Dataset-related differences explain only 11% of the variance; non-thermal effects explain up to 13% of the variance. We address the paucity of benthic data, establishing with more certainty that temperature sensitivity is indistinguishable from planktics and inorganic calcite. The large benthic dataset resolves a previously uncharacterized correlation with $[CO_3^{2-}]$ that is small ($\Delta\Delta_{47}/\Delta CO_3^{2-}$ slope = 0.00019 ±0.00004, n = 66; R^2 = 0.315, p <0.01). We report a multivariate regression to account for both temperature and $\Delta[CO_3^{2}]$ for all benthics (epifaunal and infaunal), with $\Delta_{47} = 0.152 \pm 0.049 + 0.03865 \pm 0.00376 \times 10^6/T^2 + 0.000150 \pm 0.0000601 \Delta[CO_3^{2-}]$. We apply these regressions to published Cenozoic benthic Δ_{47} data, with the multivariate benthic equation yielding temperature and $\delta^{18}O_{sw}$ values more consistent with independent proxies, models, and the broader understanding of ocean and cryosphere dynamics under different conditions, including across the Eocene-Oligocene Transition and the Early Eocene Climatic Optimum. In total, this work enables the application of clumped isotopes to foraminifera with a more realistic understanding of uncertainties.

Plain Language Summary

Carbonate clumped isotopes (Δ_{47}) is an emerging proxy for temperature. Several calibration studies have examined the relationship between Δ_{47} and temperature in core-top foraminifera but have used small datasets. Here we measure new samples and restandardize published data for foraminifera and synthetic calcite using best practices and explore controls on the proxy using results for 260 samples (>2500 analyses). We confidently demonstrate with a large dataset that foraminiferal Δ_{47} shows a temperature dependence like inorganic calcite, report a robust temperature calibration relationship, and discuss evidence for a possible carbonate ion effect on benthic foraminifera that merits further examination. We then apply the new calibrations to address some puzzling aspects of published Cenozoic benthic foraminiferal temperature and $\delta^{18}O_{sw}$ reconstructions.

1 Introduction

Accurate constraints on past ocean temperatures are critical to understanding ocean-climate interactions and Earth's climate history. However, employing proxies for temperature requires frameworks for disambiguating thermal effects from chemical, biotic, and/or diagenetic imprints. Therefore, a large body of work has focused on calibrating and applying temperature proxies, including $^{18}O/^{16}O$ ratios ($\delta^{18}O$) in foraminifera (Zachos et al., 1994, 2001, 2008), Mg/Ca (Anand et al., 2003; Elderfield and Ganssen, 2000; Lea et al., 1999; Haynes et al., 2023; Mashiotta et al., 1999; Nürnberg et al., 1996; Pak et al., 2004), the alkenone unsaturation index (Conte et al., 2001, 2006; Müller et al., 1998; Sachs et al., 2000), and TEX_{86} (Kim et al., 2008; Leider et al., 2010; Powers et al., 2010; Schouten et al., 2007; Tierney and Tingley, 2014). Each of these approaches leverages a temperature tracer recorded in sedimentary material and compounds produced by different types of organisms. Although each temperature proxy has been applied to provide information on the history of the oceans (e.g., Bard, 2000; Bard et al., 1997; de Garidel-Thoron et al., 2005; Koutavas, 2002; Lea et al., 2002; Martin and Lea, 2002), limitations exist, such as kinetic effects, unconstrained species-specific vital effects, the need for regional and latitudinal specific calibrations, the influence of changing seawater chemistry, and/or poor preservation potential.

More recently, a temperature proxy has emerged as a potentially transformative tool in the ocean sciences is carbonate clumped isotope thermometry, which may be robust to some of these limitations (Came et al., 2007; Ghosh et al., 2006; Leutert et al., 2019; Meckler et al., 2022; Meinicke et al., 2020; Peral et al., 2018; Piasecki et al., 2019; Thiagarajan et al., 2011; Tripati et al., 2010, 2014). The clumped isotope thermometer stands out because of its basis in thermodynamics (Ghosh et al., 2006; Schauble et al., 2006; Tripati et al., 2015). In calcite, aragonite, dolomite, other carbonates, and different chemical species of dissolved inorganic carbon (DIC), heavier isotopes of C and O (^{13}C, ^{18}O) are rare relative to the lighter isotopes (^{12}C, ^{16}O). Carbonate "clumped" isotope geochemistry examines the proportion of these heavy isotopes that are bound to each other forming heavy isotope "pairs" or clumps, for example, the multiply-substituted isotopologues $^{13}C^{18}O^{16}O$ (the predominant species used for temperature reconstructions, to date) or $^{12}C^{18}O^{18}O$.

Since the first studies of clumped isotope systematics in foraminifera were published (Grauel et al., 2013; Tripati et al., 2010), the use of the temperature proxy in paleoceanography has been limited because of the large sample sizes needed for the analyses (Table 1), and the presence of interlaboratory offsets (see

Bernasconi et al., 2018, 2021; Dennis et al., 2011; Petersen et al., 2019; Tang et al., 2014 for discussion). The work of multiple labs has been addressing these issues, including the use of consistent standardization and more accurate methods for isotope ratio calculations (Dennis et al., 2011; Bernasconi et al., 2021; Daeron et al., 2016; Upadhyay et al., 2021; Lucarelli et al., 2023) and sample size reduction (Grauel et al., 2013; Upadhyay et al., 2021). Building on these advances, downcore records have been published for foraminifera (e.g., Tripati et al., 2014; Leutert et al., 2019; Meckler et al., 2022).

However, recent work has highlighted the need for additional work to improve clumped isotope calibrations for foraminifera, particularly for benthics (Daeron and Gray, 2023; Rohling et al., 2024). To date, the exploration of potential chemical and biological biases has been limited, and the scope of non-thermal effects that we know confound other proxies are unresolved for clumped isotopes. For example, studies have shown for oxygen isotopes and Mg/Ca ratios in foraminifera, carbonate ion effects can be important (Bemis et al., 1998; Elderfield et al., 2006; Saenger and Evans, 2019; Spero et al., 1997).

Thus, in this study, we build on these developments in the systematics of other proxies to similarly advance the foundation for more widespread use of clumped isotope thermometry in foraminifera as a tool in paleoceanography. We recognize that a key aspect underpinning the nuanced application of temperature proxies has been the development of large datasets (Anand et al., 2003; Elderfield et al., 2006), as well as meta-analysis (e.g., Bemis et al., 1998; Daeron and Gray, 2023; Elderfield et al., 2006) to allow for the intensive characterization of thermal and non-thermal effects to understand the circumstances in which proxy application may be limited. Therefore, here we utilize current analytical methods and report new Δ_{47} data for 124 core-top foraminiferal samples, including data on previously unstudied species. Next, we reprocess data from published studies on foraminiferal samples (n = 136) using updated data handling practices including use of the IUPAC parameter set (Daëron et al., 2016; Petersen et al., 2019), and carbonate-based standardization onto the Intercarb-Carbon Dioxide Equilibrium Scale (I-CDES or I-$CDES_{90}$) reference frame (Bernasconi et al., 2021; Lucarelli et al., 2023; Upadhyay et al., 2021). These data were generated on multiple models of mass spectrometer and carbonate preparation systems and together allow us to report a novel combined dataset. We report a combined benthic foraminiferal dataset that is composed of 42 monospecific samples and 25 mixed benthic foraminiferal samples. We conduct a meta-analysis to assess if there are interlaboratory related effects or other non-thermal effects, including evidence for ecological, taxonomic, regional, or depth-dependent isotope effects. We derive calibrations for planktic and benthic foraminifera (and different subsets of these taxa) and compare them to synthetic calcite. We use this dataset to determine benthic multivariable regressions that account for a dependence of Δ_{47} on both temperature and $\Delta[CO_3^{2-}]$. These calibrations are used to reevaluate published reconstructions of deep ocean temperature from $\delta^{18}O$ and Δ_{47}.

1.1 Background on clumped isotope thermometry

Carbonate clumped isotope thermometry has the potential in paleoceanography to be similarly impactful as oxygen isotope thermometry. For over 50 years, the primary isotopic tool used to constrain past ocean temperatures has been the $\delta^{18}O$ of foraminifera (Shackleton and Opdyke, 1973; Zachos et al., 1994, 2001, 2008). For example, foraminiferal $\delta^{18}O$ has been used to provide critical constraints on how temperature, ice volume, salinity, water column structure, and ocean circulation have responded to past changes in greenhouse gas concentrations. However, a long-standing challenge in such applications has been accurately partitioning the thermodynamic fractionation of oxygen isotopes in carbonates from the effects of changing water $\delta^{18}O$. In contrast, carbonate clumped isotope thermometry is not sensitive to water $\delta^{18}O$. All that is needed to determine mineral formation temperatures is the clumped isotope composition of the solid, not the water from which it grew.

Clumped isotope thermometry relies on internal isotopic exchange between isotopes in a single phase, instead of relying on an isotopic exchange reaction between different phases (e.g., $CaCO_3$ and H_2O for the carbonate-water oxygen isotope thermometer). As with oxygen isotope thermometry, zero-point energy differences between isotopic species (or isotopologues) form the basis of the clumped isotope thermometer. For carbonate minerals that have grown in equilibrium, the paired measurement of clumped isotopes and $\delta^{18}O$ in carbonate minerals can therefore yield both carbonate formation temperature and fluid $\delta^{18}O$. However, the low abundance of clumped (multiply-substituted) isotopologues ($^{13}C^{18}O^{16}O$ and $^{12}C^{18}O^{18}O$, for example), and the low temperature sensitivity of the relevant isotope exchange reactions, measurements need to be made with high precision and accuracy. Further, robust application of the geothermometer necessitates mineral equilibrium being achieved and reliable quantification of temperature dependencies, and if appropriate, corrections for kinetic isotope effects.

An initial study of clumped isotopes in planktic and benthic foraminifera and coccoliths was published four years after the geothermometer was developed (Tripati et al., 2010). Using error-in-variable regression models (a Deming regression), this study found no evidence for differences between synthetic calcite and foraminifera calibrations, nor between cultured coccolithophores and inorganic calcite, and did not find discernible taxon-specific fractionations (Tripati et al., 2010). Several calibration studies have validated those initial findings and have also made instrumental advancements by reducing sample requirements and using different methods and instrumentation for sample analysis as well as different regression models (Meinicke et al., 2020; Peral et al., 2018; Piasecki et al., 2019). Multiple studies have evaluated different models for estimation of seawater calcification temperature (e.g., Daëron and Gray, 2023; Tripati et al., 2010). Although foraminiferal measurements are challenging, there is a growing literature of applied studies using clumped isotope thermometry to reconstruct ocean temperature and $\delta^{18}O$ (e.g., Agterhuis et al., 2022; Evans et al., 2018; Leutert et al., 2019, 2020; Meckler et al., 2022; Tripati et al., 2014; Taylor et al., 2023).

1.1.1 Challenges in applying clumped isotopes to foraminifera

While the growing body of work is demonstrating the power of clumped isotope thermometry when applied to foraminifera, proxy use in paleoceanography is still limited because of several issues. Recent major technological advances in applying this proxy to foraminifera have resolved the issue of large sample sizes (Table 1). While initially 3-8 mg $CaCO_3$ were used to perform a single replicate analysis and at least three replicates required, with typical sample sizes of 9 to 30 mg (Ghosh et al., 2006; Tripati et al., 2010), a major step forward has involved reduction in sample sizes that are similar to Mg/Ca analyses with 0.1 to 0.5 mg required for a single replicate, and 3 to 50 replicates, with typical total sample sizes of 2.5 to 5 mg (Table 1). These small sample measurements (total sample sizes of 2.5 to 5 mg, including replicates) have been made on a MAT 253 isotope ration mass spectrometer (IRMS) with a kiel device (Grauel et al., 2013; Meckler et al., 2014; Meinecke et al., 2020, Piasecki et al., 2019), the Nu-Perspective IRMS and NuCarb or in-house carbonate reaction and purification devices (Anderson et al., 2021; Defliese and Tripati, 2020; Upadhyay et al., 2021). These advances make employment of the proxy on foraminifera more feasible.

For carbonate-hosted tracers, it has also been important for the community to investigate inter-lab differences (Greaves et al., 2008; Rosenthal et al., 2004) and understand whether they are associated with sample preparation or with the specific analytical technique used (Barker et al., 2003, 2005; Bian and Martin, 2010; Martin and Lea, 2002). In clumped isotopes, interlaboratory offsets have been reduced through updated data handling practices including use of the IUPAC parameter set (Daëron et al., 2016; Petersen et al., 2019), and carbonate-based standardization onto the I-CDES reference frame (Bernasconi et al., 2021; Lucarelli et al., 2023; Upadhyay et al., 2021; Anderson et al., 2024).

1.2 Overview of this study

In this study, we leverage advances, best practices, and instrumentation that have been shown to yield highly precise, accurate, and intercomparable data (Bernasconi et al., 2021; Upadhyay et al., 2021; Lucarelli et al., 2023; Daeron and Gray, 2023). First, we utilize current analytical methods that have been shown to yield highly precise, accurate, and intercomparable data, with all data reported on the I-CDES reference frame (Bernasconi et al., 2021; Upadhyay et al., 2021; Lucarelli et al., 2023). We report Δ_{47} data for new foraminiferal samples (n = 124; 82 planktic foraminiferal samples and 42 benthic foraminiferal samples) which includes data on previously unstudied species. We reprocess data from published studies on foraminiferal samples (n = 136) using different types of instrumentation. This facilitates a substantial combined dataset comprised of 260 core-top planktic and benthic foraminiferal samples, with 29 species and 2569 replicate analyses, from several major ocean basins (Table 1).

Figure 1. Locality information for core-top samples used in this study. Map shows sites and histogram shows water depths. Site information is in Table S1.

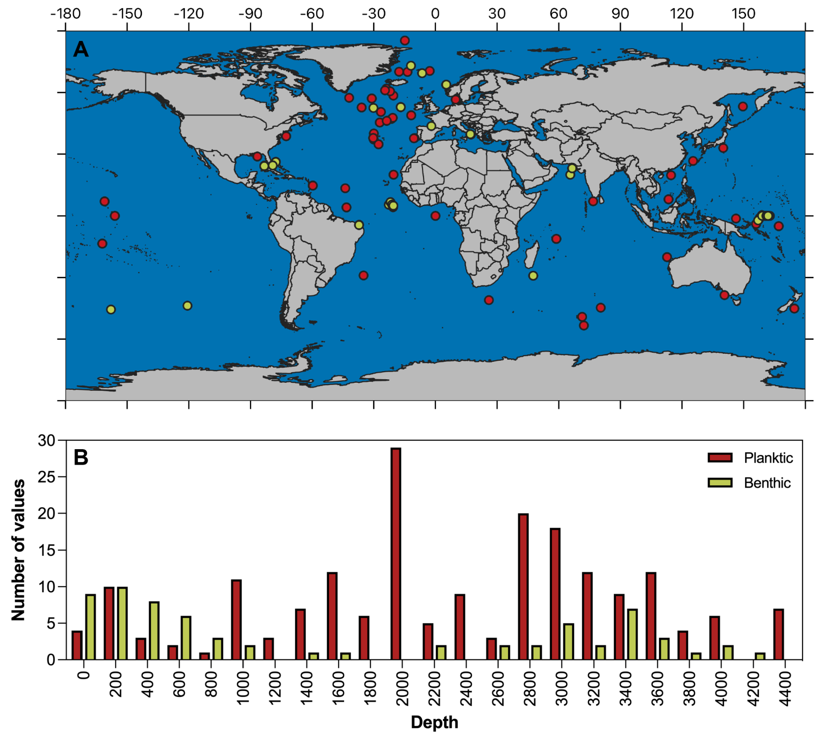

We evaluate the use of multiple calcification temperature methods, including different δ^{18}O-based calcification temperature equations. We conduct a meta-analysis to assess if there are interlaboratory related effects or other non-thermal effects, including evidence for ecological, taxonomic, regional, or depth-dependent isotope effects, and show non-thermal effects can explain only 13% of the data variance. We derive calibrations with significant data representation for both planktic and benthic foraminifera - where previously relatively little benthic data has been published - and compare results to synthetic calcite. We derive Δ_{47}-temperature calibrations for foraminiferal samples to compare material specific differences and report limits for accuracy and precision of reconstructions. We validate prior findings of no significant deviation from foraminiferal test Δ_{47} temperature sensitivity to inorganic calcite precipitates (118 samples; 641 analyses; grown in experiments at temperatures between 4 and 50 °C; Table 2). The analysis of benthic foraminiferal data indicates a weak carbonate ion effect, and we report a new multivariate regression relating Δ_{47} to both temperature and carbonate saturation. Finally, we apply our novel calibrations. We analyze profile temperature reconstructions and show that modern hydrographic profiles are reasonably constrained using data from multiple taxa, show the impact of the use of our new calibrations on reconstructed temperatures on Cenozoic temperatures, and make recommendations for future studies.

2 Materials and Methods

2.1 Sample and locality information

Samples are from the four major ocean basins (Arctic, Atlantic, Indian, Pacific), the Gulf of Mexico, and the Mediterranean Sea (Figure 1, Table S1). Figure 1 shows locality information for the 49 sites. A total of 29 foraminifera taxa were studied (13 benthic, 15 planktic), and assemblages of mixed benthic species. The species included in this study live in a range of habitats, spanning Atlas temperatures from -1.5 °C to 29.6 °C (Levitus et al., 2010). Data for 124 foraminifera samples are newly reported and were run in the Eagle-Tripati clumped isotope laboratory at UCLA, while 136 samples from five previous publications (Breitenbach et al., 2018; Meinicke et al., 2020; Peral et al., 2018; Piasecki et al., 2019; Tripati et al., 2010) were projected into the I-CDES reference frame for this work (Table 1, Table S2).

Table 1. Sources of clumped isotopic data from foraminifera used in this study. Data for 260 core-top foraminifera are reported (based on 2569 analyses), comprised of 124 new foraminifera samples measured for this study, and 136 samples reported in prior publications (Tripati et al., 2010; Peral et al., 2018; Breitenbach et al., 2018; Meinicke et al., 2020; Piasecki et al., 2019). The dataset from Grauel et al. (2013) was excluded based on the PI from the measuring laboratory not being confident in the standardization of the dataset. Coccolith bulk measurements from Tripati et al. (2010) were not included in this study. Foraminifera calcification temperatures are recalculated with multiple methods as described in section 2.4.2. All published datasets were updated to the same standardization reference frame (I-$CDES_{90}$).

Publication	Ecology	# samples	# of analyses	Mass/replicate (mg)	# replicates	Integration time (seconds)
Tripati et al., 2010	planktic, benthic	34	58	4-8	1-5	640-1280
Grauel et al., 2013	planktic, benthic	42	618	0.15-0.2	2-47	156
Peral et al., 2018	planktic, benthic	27	248	2-3	4	480
Breitenbach et al., 2018	planktic	19	158	0.12-0.24	1-12	208
Meinicke et al., 2020	planktic	43	830	0.1-0.13	15-30	400
Piasecki et al., 2019	benthic	13	582	0.1-0.4	1-43	400
This study New measurements	planktic, benthic	124	720	0.25-0.52	3-20	1200
This study Foraminifera meta-analysis	**planktic, benthic**	**260**	**2569**			

2.2 Methods for new samples measured in the Eagle-Tripati laboratory

2.2.1 Sample Preparation

Core-top sediment samples from 47 different sites were suspended in deionized (DI) water for a minimum of 24 hours using a rotating wheel (Table S1). Fine and coarse fraction were separated using a 63 µm sieve and dried overnight at 30 °C (≤ 50 °C to prevent bond reordering). A total of 16 different taxa, both planktic and benthic, and mixed benthic species, were hand-picked from different size fractions at these sites. Tests were translucent and intact. We aimed for a minimum weight of picked foraminifera of 3 mg to have sufficient material for several replicate analyses.

Picked samples underwent a cleaning procedure to remove potential contaminants, adapted from the cleaning procedure for Mg/Ca analysis from Barker et al. (2003), as described in Tripati et al. (2010), with a focus on removing infill and adhering sediment. Briefly, foraminiferal shells are cracked open, rinsed and ultrasonicated using methanol and DI water until the cleaning water is clear. Each ultrasonication step consisted of 4 intervals lasting 15 seconds to ensure that the water did not heat up. Samples were then placed inside an oven to dry overnight at 30 °C (< 50 °C). Samples were homogenized using a mortar and replicates were weighed and stored in a desiccator until the day of analysis. Additional details on sample preparation are provided in the Supplement (S2).

2.2.2 Measurement Procedure

Aliquots of cleaned samples that ranged from 0.46 to 0.52 mg were measured in single analyses, with 3 to 20 replicates measured per sample. A total of 720 new analyses of 124 foraminifera samples were made. Samples were analyzed from 2017 to 2023 on two Nu Perspective Dual inlet mass spectrometers with secondary electron suppression. These were run on instrument configurations "2" (Nu Perspective

2014, acid bath 90 °C), “3A” (Nu Perspective 2014, Nu Carb, 70 °C) and “3B” (Nu Perspective 2016, Nu Carb, 70 °C) that were shown in Upadhyay et al. (2021) and Lucarelli et al. (2023) to yield statistically indistinguishable results from each other.

Every 4 to 5 sample measurements, a carbonate standard was measured and Δ_{47} values are reported on the Inter-Carbon Dioxide Equilibrium Scale (I-CDES$_{90}$, Bernasconi et al. 2021) at 90 °C. A total of seven standards were used, including ETH-1, ETH-2, ETH-3, ETH-4, CM Tile, Carmel Chalk, and Veinstrom (Upadhyay et al., 2021; Lucarelli et al., 2023). ETH-1 and ETH-2 were used for non-linearity corrections while ETH-1, ETH-2, and ETH-3 and the remaining in-house standards were utilized for $\delta^{13}C$ and $\delta^{18}O$ drift corrections and empirical transfer function (ETF) calculations. ETH-4 was used as a consistency standard and not included in any standard corrections. Depending on standard drift during a correction interval, we utilized either 10 or 20-point moving averages for drift, nonlinearity, and empirical transfer function corrections for each correction interval, following published studies (Meckler et al., 2014; Upadhyay et al., 2021; Lucarelli et al., 2023). The Brand parameter set was used for calculations (Daëron et al., 2019; Petersen et al., 2019). Calculations to determine Δ_{47}, $\delta^{13}C$, and $\delta^{18}O$ use publicly available software (Easotope - John and Bowen, 2016) and further details on clumped isotopes are provided in the Supporting Information (Section S1).

2.2.3 Accuracy and precision of data and data archiving

Standard values for each instrumental configuration are typically within 0.005‰ of values reported by Bernasconi et al. (2021) as described in Upadhyay et al. (2021) and Lucarelli et al. (2023). Long-term absolute mean error in standard Δ_{47} across instruments is 0.0002‰ (or 0.03% in percent terms), and is normally distributed (Upadhyay et al., 2021; Lucarelli et al., 2023). The average Δ_{47} standard deviation (1 s.d.) among standard replicates for all instruments is 0.021‰ (Upadhyay et al., 2021; Lucarelli et al., 2023).

Similar values are reported for samples. For samples, average Δ_{47} reproducibility is 0.022‰ (1 s.d.) and 0.009‰ (1 s.e.) Supporting Information Table S1). The ranges for samples are 0.001-0.049‰ (1 s.d.) and 0.000-0.029‰ (1 s.e.). Standard and sample data for new measurements are provided using the recommended EarthChem template (Petersen et al., 2019) and archived online with manuscript acceptance.

2.2.4 Quality control

Data quality control followed published procedures described in Parvez et al. (2023). Although in the laboratory, samples are routinely screened based on Δ_{48} or Δ_{49} values that are indicative of high organic content, all samples reported for this study fell within initial screening bounds, so no replicates were excluded based on this criteria. Replicates with incomplete gas transfer and Δ_{47}, $\delta^{13}C$, and $\delta^{18}O$ values that fall outside of a SD range of ±0.5‰ for $\delta^{13}C$ and $\delta^{18}O$ and ±0.05‰ for Δ_{47} are also flagged. Similar screening thresholds for Δ_{47} were reported by Meckler et al. (2014), Upadhyay et al. (2021), and Lucarelli et al. (2023). Data were screened based on instrument source stability, pumpdown times and leaks in the acid digestion system, and standard data quality during correction intervals as described in Parvez et al. (2023). Of the new analyses conducted for this study, 720 replicates were included, and 52 replicates excluded.

2.3 Reprocessed datasets from publications

2.3.1 Core-top foraminiferal datasets

Five published foraminiferal datasets (Breitenbach et al., 2018; Meinicke et al., 2020; Peral et al., 2018; Piasecki et al., 2019; Tripati et al., 2010) were reprocessed onto the I-CDES$_{90}$ reference frame as part of this study. The foraminiferal data include 24 different taxa (10 benthic, and 14 planktic) and mixed benthic samples from Tripati et al. (2010) and Piasecki et al. (2019) (Table 1, S2, S3). After discussion with S. Bernasconi about Grauel et al. (2013) and the reprocessing of their dataset, data from the study were not included, as the measurements only included the use of two marble (high-temperature) standards with low Δ_{47} values, with no carbonate standard with high Δ_{47} values used for their corrections.

2.3.2 Synthetic calcite datasets

We compare our foraminiferal data to synthetic calcite to assess if there are differences between the two groups. Since growth temperatures for foraminiferal samples occupy a much narrower range of temperature than many synthetic calcite precipitates used for calibration purposes, we limit the data used for synthetic calcite to 4 to 50 °C.

A total of 118 synthetic calcite samples comprising 641 replicates were utilized for this comparison: we include 11 new measurements of synthetic calcite analyzed in the same manner as foraminiferal samples on the I-CDES$_{90}$ reference frame (Table 2, Supporting Information Table S4), 19 samples were reprocessed as part of this study (Defliese and Tripati, 2020; UCLA samples from Tang et al., 2014; Tripati et al., 2015) and 85 additional synthetic calcite samples from other studies (Table 2, Supporting Information Table S4). Synthetic calcite calibration samples from other studies include samples that were reprocessed using Brand parameters in the Petersen et al. (2019) study (Defliese and Lohmann, 2015; Kelson et al., 2017; Kluge et al., 2015; Tulane samples from Tang et al., 2014), as well as Anderson et al. (2021), Lucarelli et al. (2023), Jautzy et al. (2020), and Swart et al. (2021).

Table 2. Sources of clumped isotopic data from synthetic calcite used in this study. Data for 118 samples of synthetic calcite grown from 0 to 50 °C are reported (based on 641 analyses), comprising 11 new samples measured for this study, and 104 samples reported in prior publications. All published datasets were updated to the same standardization reference frame (I-CDES$_{90}$).

Publication	# samples	# analyses	Mass/replicate (mg)	# replicates	Integration time (seconds)
Anderson et al., 2021	10	87	0.4 - 0.6	8-10	1800
Defliese et al., 2015	3	12	4-6	4	640
Defliese and Tripati 2015	2	19	0.25-0.5	7-12	640-1600
Jautzy et al., 2020	4	85	0.08 - 0.1	19-24	700
Kelson et al., 2017	30	108	6-9	2-7	1560
Kluge et al., 2015	6	18	5 – 8	1-5	1456
Lucarelli et al., 2022	4	36	0.48-0.52	5-12	1200
Swart et al., 2021	6	73	5-8	3-14	2436
Tang et al., 2014	32	101	25	1-24	1200
Tripati et al., 2015	7	13	5 – 8	1-4	1200
This study New measurements	11	89	0.48 - 0.52	6-13	1200
This study Synthetics meta-analysis	**115**	**641**			

2.3.3 Data reprocessing for published datasets

The Tripati et al. (2010) dataset for foraminifera and Tripati et al. (2015) dataset for synthetic calcite were reprocessed for use in this study in the Easotope software (John and Bowen, 2016) with updated parameter values (Daëron et al., 2016) and standard values (Bernasconi et al., 2021; Lucarelli et al., 2023) on the CDES absolute reference frame. Gas standards are used for the nonlinearity correction step and a combination of gas and carbonate standards for the ETF to project onto the CDES reference frame (see methods section 2.1.2). We use these new Δ_{47} (CDES) values, along with the transfer functions (Supporting Information Table S5) constructed from Bernasconi et al. (2021) to project values into the I-CDES$_{90}$ reference frame.

We also reprocessed data from the Petersen et al. (2019) study (Defliese et al., 2015; Kelson et al., 2017; Kluge et al., 2015; Tang et al., 2014). These datasets were initially brought onto the CDES reference frame at 25 °C (Dennis et al., 2011) using ETH carbonate standards (Bernasconi et al., 2018) and acid fractionations associated with Brand parameters (Daëron et al. 2016). We use these originally published Δ_{47} CDES values in concert with the methodology described in Bernasconi et al. (2021) to project values into the I-CDES$_{90}$ reference frame.

We reprocessed data from Defliese and Tripati (2020) and Tang et al. (2014) that were measured at UCLA as part of this study in Easotope on I-CDES$_{90}$. Data from Anderson et al. (2021), Lucarelli et al. (2022), Jautzy et al. (2020), and Swart et al. (2021) were already in I-CDES$_{90}$ and were not reprocessed.

2.4 Ecological and Hydrographic data

Foraminiferal Δ_{47} values were compared to estimates of calcification temperature, that in turn are constrained by independent datasets (i.e., habitat, ocean atlas-derived calcification temperatures, oxygen-isotope derived calcification temperatures). We also use multiple methods to probe secondary (non-thermal effects). We use Δ_{47}-temperature regression models to estimate vertical profiles of temperature and compare results to ocean atlas temperatures.

2.4.1 Habitat

Species were classified by depth habitats including mixed-layer, mixed-layer to thermocline, and thermocline for planktic species, and epifaunal and infaunal for benthic species. Specific depth habitats and ranges for different taxa were taken from Rippert et al. (2016) and Schiebel and Hemleben (2017) and references therein. We note that calcification depths of foraminifera vary seasonally and can evolve with ontogeny, as well as depend on factors influencing feeding patterns (Schiebel and Hemleben, 2017). Ocean basins sampled in the complete dataset include the Arctic, Atlantic, Indian, and Pacific Oceans, as well as the Mediterranean Sea and the Gulf of Mexico.

2.4.2 Calcification temperatures

Calcification temperatures for each sample were calculated for new and reprocessed samples, so that we could ensure the same methods were consistently used (Supporting Information Table S3). Three methods were utilized and a comparison of results is provided in the Supporting Information material (Section S3). Briefly, method 1 uses the literature on calcification depths of foraminifera species in geographical regions in conjunction with WOA temperature data (version 13V2; Levitus et al., 2010) to estimate calcification temperatures. Method 2 consists of combining measured $\delta^{18}O$ of foraminiferal tests with seawater $\delta^{18}O$ (at assumed foraminiferal calcification depths and growth seasons) from a database (LeGrande and Schmidt, 2006), in combination with published taxon-specific $\delta^{18}O$-temperature relationships. For the latter, we referred to the most data-rich study on planktic taxon-specific $\delta^{18}O$-temperature relationships from Malevich et al. (2019) that compiles data from >2600 core top samples from five taxa and reports Bayesian regression models that are taxon-specific as well as a pooled calibration. They examined both annual and seasonal data, with similar errors for each. For our calcification temperature estimates, in the case of taxa for which species-specific calibrations were provided, we used the seasonal hierarchical model to estimate calcification temperatures and used the pooled calibration for all other planktic species. To estimate calcification temperatures of benthic taxa, we implemented equation 9 of Marchitto et al. (2014) for epifaunal species and mixed benthics, and the same equation modified by 0.47 ‰ for infaunal species as the authors suggest. Method 2, presented in the figures and the text, uses assumed calcification depths and oxygen isotope measurements, to estimate calcification temperatures for planktic foraminifera. Additionally, isotopic calcification temperatures were estimated using Method 2, but with equations from Kim and O'Neil (1997) and Shackleton (1974). Method 3 uses theoretical values of $\delta^{18}O_{calcite}$ to develop vertical profiles and compares them to measured $\delta^{18}O_{calcite}$ values to determine the minimum and maximum calcification depths.

2.4.3 Salinity

Estimated salinity is calculated using published decadal averaged seawater salinity from the WOA18 gridded dataset (Zweng et al., 2019). Salinity is averaged for each species at each site over their site-specific assumed calcification depths.

2.4.4 Bottom water saturation state

Bottom water saturation state was compared to benthic foraminiferal data to assess carbonate ion effects on calcification, with the caveat that infaunal taxa may inhabit environments with values that differ in composition from bottom waters. For these comparisons, calcite saturation state ($\Delta[CO_3^{2-}]$) is calculated as the difference between the in-situ carbonate-ion concentration ($[CO_3^{2-}]$) and the carbonate-ion concentration at saturation ($[CO_3^{2-}]_{sat}$). Carbon system data was obtained from the nearest neighbor sites from the World Ocean Circulation Experiment and the Global Ocean Data Analysis Project (Olsen et al., 2019) and carbonate-ion concentration was calculated via Ocean Data Viewer (http://woce.nodc.noaa.gov/wdiu) using best practices by Dickson et al. (2007).

2.5 Statistical Models

We used multiple statistical methods for this work. One method was used for developing regressions between Δ_{47} and temperature. Multiple approaches were applied for comparing subsets of data to assess if different models are needed (i.e., for foraminifera relative to synthetic calcite, or planktics relative to benthics). We used different approaches to assess if non-thermal effects are substantial (i.e., carbonate ion effects).

2.5.1 Regressions between Δ_{47} and calcification temperature

We fit regressions between Δ_{47} and calcification temperature utilizing Deming models. Among multiple analyzed frequentist regression models, Deming models are known to outperform other errors in variable models (i.e., York models), with higher levels of accuracy and precision for datasets of these sizes and similar error structures (Román-Palacios et al., 2021). Regression parameters from these models are generally congruent with Bayesian-derived estimates (Román-Palacios et al., 2021). We use Deming models to investigate potential non-thermal effects and differences between data subsets through confidence interval (CI) comparison.

2.5.2 Use of R-based model selection for investigation of non-thermal effects

We used a model selection approach to determine whether non-thermal factors substantially impact isotopic signatures in foraminifera. Deming regressions are strictly univariate, so we substituted multivariate ordinary least squares (OLS) linear models in R version 4.1.2 (R Core Team, 2022). The potential suite of non-thermal variables consisted of lab/dataset, salinity, depth, region, photosymbiont presence, habitat, genus, ocean, and bottom water saturation state. Because this constitutes a large number of potential variables (set within a model as predictor variables) that could feasibly impact the final Δ_{47} value, with an unknown potential for interactions between variables, we employed automated model selection using the multithreaded implementation of the 'dredge' function in R package MuMIn version 1.47.1 (Bartoń, 2022). All numerical predictor variables were scaled and centered (i.e., z-scored) prior to building models, as differences in the absolute magnitude of predictor variables can lead to erroneous results in effect size calculations. Scaling the response variable was found to be unnecessary.

We report coefficients from linear models fit to z-scored data, which provides an estimate of the per mil change in Δ_{47} for each 1 standard deviation (1 σ) increase in the predictor variable(s) of interest. Uncertainty around coefficients is given in standard error in permil units. The effect size, partial eta squared (η^2), is used to evaluate how much variation in foraminiferal Δ_{47} is explained by each model component (fit to z-scored data) and determine whether those effects are small (partial η^2 = 0.01), medium (partial η^2 = 0.06), or large (partial η^2 >= 0.14) when all other variables in the model are held constant. The calculation for η^2 is mathematically similar to the calculation for R^2 and may therefore be interpreted in a similar manner for individual model components. Note that we report effect sizes calculated using Type II (non-sequential) sums-of-squares as implemented in the *car* package for R (Fox and Weisberg, 2019). This means that the impact of each predictor variable on foraminiferal Δ_{47} is evaluated individually in turn, while all other predictor variables are held constant. Effect sizes may therefore add up to >1. As η^2 is calculated using a one-sided hypothesis, we report one-sided 95% confidence intervals. Where final models include only a single predictor variable (temperature), partial η^2 is equivalent to η^2, and so η^2 is reported. Linear model F-statistics are reported with the numerator and denominator degrees of freedom listed as subscripts in that order.

A 'full' model was constructed for each subset of data (by lab/dataset, habitat, etc.) which contained all relevant candidate predictor variables. The 'dredge' function then examined every possible combination of predictor variables and determined the most likely reduced models. Candidate reduced models were manually checked for goodness-of-fit and extraneous terms were dropped if warranted. To determine whether dropping extraneous terms improved model fit, a hypothesis testing approach, followed by examination of the Akaike Information Criterion (AIC), was used to select between the reduced model identified by 'dredge' and a simplified model with terms dropped. If hypothesis testing and AIC indicated that two reduced models were equally likely to fit the data, we defaulted to the simpler model (e.g., the model with fewer terms or without interactions). Effect sizes and confidence intervals for final model components were calculated using R package effectsize version 0.7.0.5 (Ben-Shachar et al., 2020), with non-sequential (Type II) sums-of-squares calculated in R package car version 3.1-1 (Fox and Weisberg, 2019). Full details of this method are available in the Supporting Information (Section S5). We also use OLS for directly investigating non-thermal dependences (i.e., regressions between Δ_{47} residuals and bottom water $\Delta[CO_3^{2-}]$). Individual comparisons between data subsets are done using ANCOVA-type analyses (performed in Graphpad Prism). Tests for multicollinearity confirm PCA results, with the additional ability to include categorical predictors, and show no evidence of problematic degrees of correlation between predictor variables including temperature, dataset, depth, carbonate saturation, salinity, and photosymbiont presence/absence.

2.6 Temperature reconstruction

We reconstruct temperatures using core-top data for multiple species of foraminifera at several locations to evaluate the fidelity of using this approach to constrain hydrographic profiles in different oceanographic regimes. Temperatures were estimated using the full foraminiferal regression from the meta-analysis (labelled "All Foraminifera" in Table 3).

3 Results and Discussion

3.1 Sensitivity of regression to calcification temperatures estimated using different methods

Figure 2 shows Δ_{47} values for calibration samples compared to $\delta^{18}O$-based calcification temperatures estimated using the species-specific Bayesian model (method 2). Supporting Information Table S3 contains the calcification temperature estimates from different methods, and water isotope values and the supplement compaFres results from these different methods in more detail. Briefly, although all three methods yield results that are broadly similar, there are some notable differences. Calcification temperatures derived from method 1 (the WOA13 values) show more scatter than those estimated using either methods 2 or 3 (oxygen isotope-based estimates) as is evidenced by a lower Pearson's correlation coefficient (see Supporting Information S4). Differences between the Atlas (method 1) and isotopic temperatures (method 2) reach up to 13.4 °C for the same sample, which is a *Trilobatus sacculifer* from the Equatorial Pacific from Tripati et al. (2010). In contrast, calcification temperatures derived from method 2 and method 3 yield small differences for most samples (max = 5.1 °C). Method 2 allows for the use of the species-specific Bayesian model for carbonate $\delta^{18}O$ temperature estimates and decreases the temperature estimate error for planktic samples. If we solely examine the new dataset generated at UCLA on 124 foraminiferal samples, we reach similar conclusions with the largest Pearson's correlation from Method 2 ($r = 0.898$) and relatively small differences between Method 2 and 3 (mean = 0.0077 °C, SD = 1.7 °C).

We conclude from our meta-analysis that the differences between methods are generally small, with the smallest offsets between Method 2 and Method 3 and the largest offsets between Method 1 and

Method 3. Results from Method 2 exhibited the strongest correlation between temperature and Δ_{47}, both in the new dataset generated at UCLA and the overall meta-analysis. The method is similar to what was used by Meinicke et al. (2020) and what is recommended by Daeron and Gray (2023). Given Method 2 has the strongest correlation between temperature and Δ_{47}, both in the new dataset generated at UCLA and the overall meta-analysis, it was the method utilized for calcification temperature estimation in this study.

Figure 2: Calibration data from this work, including new calibration data (blue) and a meta-analysis of all data (grey) standardized to be on the same reference frame (I-CDES). (a) New calibration data for small foraminiferal samples from the Eagle-Tripati Lab (blue; n = 124) compared to a meta-analysis of all data (grey; n = 260), (b) New foraminiferal data compared to a meta-analysis of synthetic calcite from a similar temperature range (0 to 50 °C; n = 118). Also shown are 95% confidence bands for the regressions. Individual point errors and coefficient errors are reported as SE. The regression through all foraminiferal data from UCLA (n = 124) is: $\Delta_{47} = 0.0353 \pm 0.0015\ 10^6/T^2 + 0.1973 \pm 0.0187$ while a regression for the full dataset (n = 260) is: $\Delta_{47} = 0.0374 \pm 0.0013\ 10^6/T^2 + 0.1745 \pm 0.0154$. For synthetic calcite (n = 118), the regression between temperature and Δ_{47} yields the equation with standard error: $\Delta_{47} = 0.0393 \pm 0.0014\ 10^6/T^2 + 0.1547 \pm 0.0165$. Regression parameters for all groups of data are in Table 3.

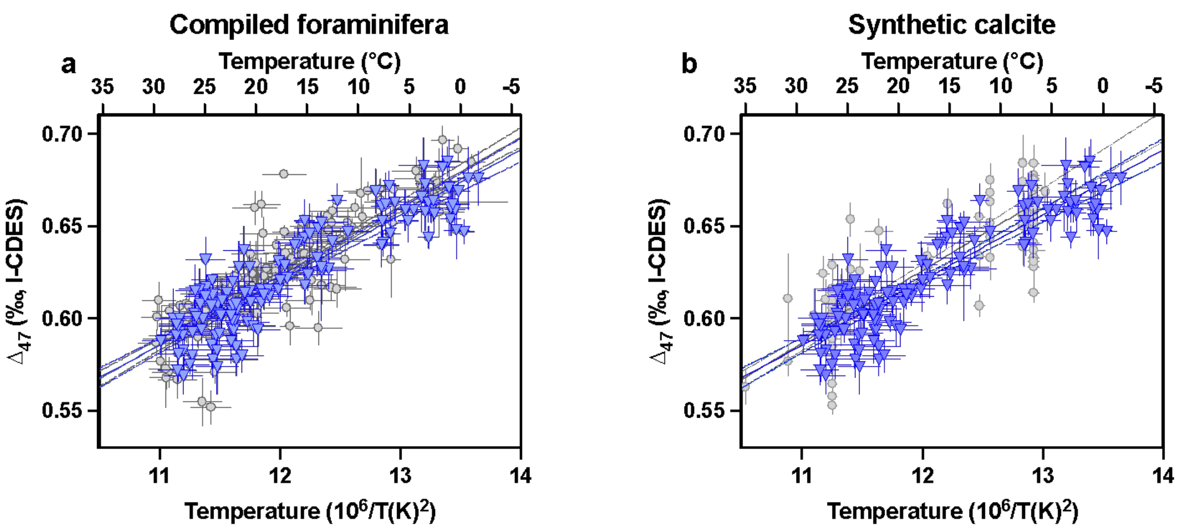

We also compare multiple models for estimating isotopic calcification temperatures utilizing Method 2. Figures S1 and S2 compare calcification temperatures for planktics (from Malevich et al., 2019) and benthics (derived from Marchitto et al., 2014) estimated using Method 2 to atlas temperatures (Method 1), and are modelled after Figure 7 from Daeron and Gray (2023). Figures S3-S6 are similar to these but utilize Method 2 but show isotopic calcification temperatures derived using the equations of Kim and O'Neil (1997) or Shackleton (1974). Figure S7 shows a histogram of the differences between isotopic temperatures and atlas temperatures. In our analysis, there are fewer benthic foraminiferal samples with large offsets between isotopic and atlas temperatures when the isotopic equation of Marchitto et al. (2014) is used (Figure S2), in contrast to when equations from Kim and O'Neil (1997) or Shackleton (1974) are utilized (Figures S4 and S6). We find the use of the temperature relationships from Malevich et al. (2019), in contrast to Kim and O'Neil (1997) and Shackleton (1974), yields relatively few planktic samples from cold waters (<10 °C) that have isotopic temperatures that are not within uncertainty of atlas temperatures (Figure S1 compared to Figures S3 and S5). At warmer temperatures, there are more planktic foraminiferal samples that are offset, irrespective of choice of $\delta^{18}O$-calibration (Figure S1); such samples are described by Daeron and Gray (2023) as being isotopically "discordant" and in this analysis, are dominated by *P. obliquloculata* and *G. ruber* (Figure S1). We speculate that the offset could reflect possible non-thermal effects on planktic foraminiferal Δ_{47}. We note that the data for *P. obliquloculata* are for sites at a range of water depths, and thus dissolution could be a contributing factor, but that is not the case for samples of *G. ruber*, as these are from shallower sites.

3.2 Δ_{47}-Temperature calibration

Figure 2 and Table 3 show the relationship between temperature and Δ_{47} for the UCLA only full foraminiferal dataset (n = 124), for the meta-analysis of the foraminiferal data, and the synthetic calcite data. Figure 3 and Table 3 also report results for different ecological subgroups of data that are well-defined (e.g., planktic, benthic, mixed-layer planktics, epifaunal vs infaunal benthics) (also reported in Supporting Information Table S5 with other subgroups of data). Results are compared to a regression for synthetic calcite grown at ≤ 50 °C (Tables 3, S3). Pearson's correlation results for all of the populations indicate a strong correlation between temperature and Δ_{47}, consistent with multiple prior studies (e.g., Ghosh et al., 2006; Hill et al., 2014; Petersen et al., 2019; Schauble et al., 2006; Tripati et al., 2015). For example, the meta-analyses of the foraminiferal data and synthetic calcite support a correlation that is significant at the >99% level (r = 0.873, t = 28.7, $p < 0.001$, and r = 0.917, t = 24.4, $p < 2.2e-16$, respectively).

Table 3: Regression parameters for foraminiferal calibration dataset and synthetic calcite dataset.

Datasets included	N	slope	s.e.	CI range	intercept	s.e.	CI range
UCLA Foraminifera	124	0.03527	0.00154	0.03222 to 0.03833	0.1973	0.019	0.1602 to 0.2344
All foraminifera	260	0.03739	0.00128	0.03487 to 0.03991	0.1745	0.015	0.1441 to 0.2049
All foraminifera, no mixed benthics	235	0.0383	0.00128	0.03579 to 0.04084	0.1635	0.015	0.13310 to 0.19390
Synthetic calcite <50 °C	118	0.03926	0.00143	0.03643 to 0.04208	0.1547	0.017	0.1219 to 0.1874
All benthics	67	0.028	0.00264	0.02267 to 0.03324	0.2948	0.034	0.2272 to 0.3625
All benthics, no mixed benthics	42	0.0342	0.00336	0.02740 to 0.04099	0.2149	0.043	0.12770 to 0.30210
All infaunal benthics	23	0.0365	0.00552	0.02505 to 0.04799	0.186	0.07	0.04126 to 0.3307
All epifaunal benthics	19	0.0317	0.00515	0.02081 to 0.04254	0.2474	0.067	0.1053 to 0.3895
All planktics	193	0.0423	0.00191	0.03854 to 0.04609	0.1166	0.023	0.07203 to 0.1612
All mixed-layer planktics	99	0.0423	0.00242	0.03746 to 0.04706	0.1194	0.028	0.063466 to 0.1754
All foraminifera and synthetic calcite	381	0.03894	0.00092	0.03713 to 0.04075	0.1566	0.011	0.1350 to 0.1782

When comparing foraminiferal results to synthetic carbonates, we see no significant differences between synthetic carbonates and foraminifera overall or between synthetic carbonates and different subgroups of foraminifera excluding mixed benthics (Figures 2 and 3, Table 3). The regression through all foraminiferal data from UCLA (n = 124) is: $\Delta_{47} = 0.0353 \pm 0.0015\ 10^6/T^2 + 0.1973 \pm 0.0187$ while a regression for the full dataset (n = 260) is: $\Delta_{47} = 0.0374 \pm 0.0013\ 10^6/T^2 + 0.1745 \pm 0.0154$. For epifaunal benthics (n = 19) the regression is $\Delta_{47} = 0.\ 0317 \pm 0.0052\ 10^6/T^2 + 0.2474 \pm 0.0674$. For infaunal benthics (n = 23), the regression is $\Delta_{47} = 0.0365 \pm 0.0055\ 10^6/T^2 + 0.186 \pm 0.0696$. For mixed layer planktics, the regression is $\Delta_{47} = 0.0423 \pm 0.0024\ 10^6/T^2 + 0.1194 \pm 0.0282$. For synthetic calcite (n = 118), the regression between temperature and Δ_{47} yields the equation with standard error: $\Delta_{47} = 0.0393 \pm 0.0014\ 10^6/T^2 + 0.1547 \pm 0.0165$.

Figure 3: Slope and intercept for Δ_{47}-temperature regressions for different data subsets from this study. Results show that regression parameters for datasets that are well constrained (i.e., taxonomically well-defined, with precise estimates of calcification temperature, and with a high n) and other datasets are indistinguishable from inorganic calcite (horizontal grey bar). These datasets include results for samples that were measured at UCLA, the full foraminiferal dataset, mixed-layer planktics, epifaunal benthics, and infaunal benthics, epifaunal and infaunal benthics, and all foraminiferal data excluding mixed benthics.

Panels A and B show slope and intercept for samples that are well constrained, respectively. Panels C and D show slope and intercept for regressions through datasets that contain more poorly constrained samples. Poorly constrained sample groups include groups with low n, groups that are taxonomically more variable, and groups that contain mixed benthic samples. 1 SE is shown in black, 95% CI in gray. Horizontal gray bar is the SE band of the synthetic regression parameters.

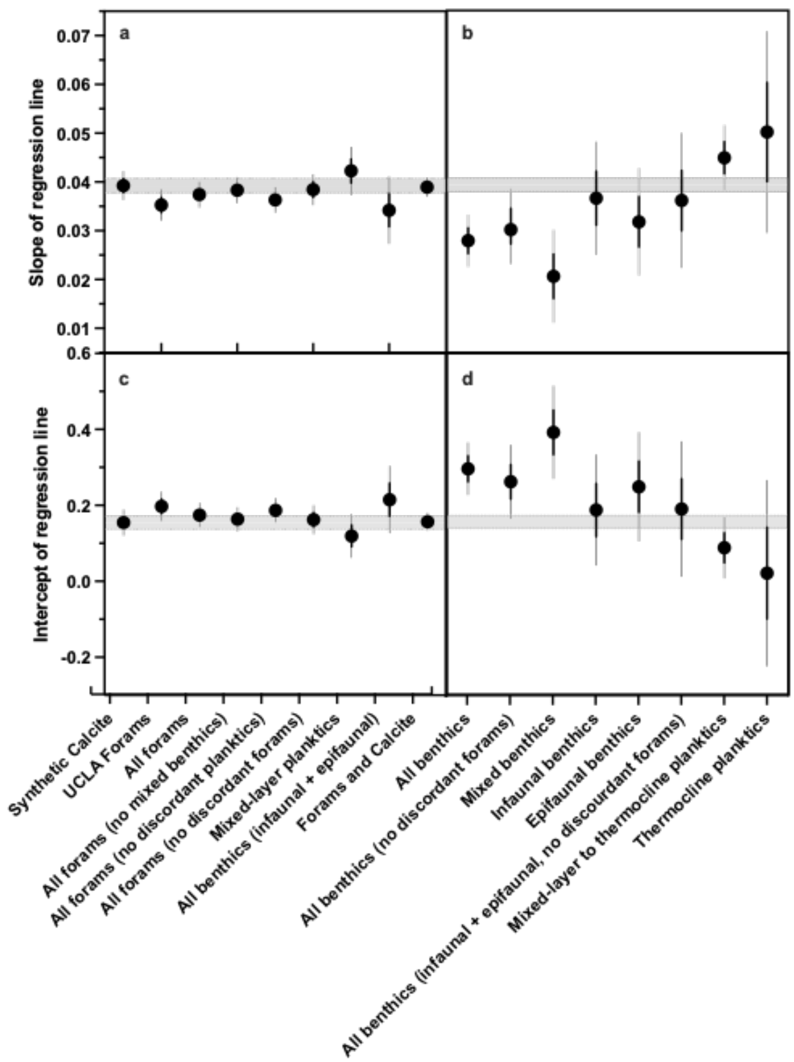

3.3 Non-thermal effects in foraminifera

To constrain the potential scope of non-thermal effects in this proxy, we build on the body of literature derived from in-depth studies of other foraminiferal proxies such as $\delta^{18}O$ and Mg/Ca (e.g., Anand et al., 2003; Gray and Evans, 2019; Lea et al., 1999; Russell et al., 2004; Stirpe et al., 2021). One group of effects are biological in origin. In some cases, taxon-specific calibrations have been argued to be a better fit (e.g., Bemis et al., 1998; Malevich et al., 2019; Skinner and Elderfield, 2005), while others suggested the use of pooled calibrations (e.g., Anand et al., 2003; Malevich et al., 2019). Recent work surveying cryptic species of foraminifera has shown there are genotype-specific biological controls on shell geochemistry, leading to suggestions that regional calibrations of proxies may also potentially be useful (Darling et al., 2017; Sadekov et al., 2016). Additionally, basinal differences have been identified for Mg/Ca (i.e., a local intercept for Mg/Ca-temperature calibration equations are adjusted to yield modern temperatures from core-top values; Skinner and Elderfield, 2005).

Seawater chemistry has been identified in some studies as being important for proxy systematics. In particular, carbonate chemistry and salinity have been described in the literature as affecting foraminiferal $\delta^{18}O$ and/or Mg/Ca. Carbonate ion effects on oxygen isotopes (Spero et al., 1997) and Mg/Ca (Lea et al., 1999; Russell et al., 2004) have been noted from culturing of planktic foraminifera. Salinity effects have also been reported on Mg/Ca (Ferguson et al., 2008; Gray and Evans, 2019; Hoogakker et al., 2009; Lea et al., 1999). Bottom water carbonate saturation is thought to impact Mg/Ca ratios in benthic foraminifera (Dawber and Tripati, 2012; Elderfield et al., 2006; Yu and Elderfield, 2008), and potentially oxygen isotopes (Bemis et al., 1998).

These factors have mostly not yet been examined for clumped isotopes in foraminifera. Studies of Δ_{47} have concluded that taxonomic effects have not been detectable (Tripati et al., 2010; Peral et al., 2018; Meinecke et al., 2020, Daëron and Gray, 2023). Similarly, carbonate ion effects have been explored in benthic foraminifera in two studies using relatively small sample sizes; they were not detectable (Tripati et al., 2010; Piasecki et al., 2019). Another study probed for and found no evidence for salinity effects in foraminifera (Peral et al., 2018). The potential scope of carbonate ion and salinity effects in foraminifera has been explored with theory and the mechanisms associated with clumped isotope effects linked to DIC speciation shown to, in principle, be limited across most oceanic conditions (Hill et al., 2014; Tripati et al., 2015). Thus, we hypothesize that non-thermal effects are likely to be weak.

3.3.1 Methodological

Our meta-analysis shows that despite methodological differences, for foraminiferal data, there is strong agreement between most labs when data are placed on the I-CDES reference frame. Clumped isotope measurements involve examination of low abundance isotopic species, and thus are counting statistics limited, and necessitate accurate and precise measurements. Thus, part of our work for this study has involved recalculating available data determined using different methods on the same I-CDES reference frame using published standard values.

Between studies, the instrumentation used varies – including carbonate digestion systems and associated reaction temperatures, mass spectrometers (with distinct signal to noise, and mass spectrometric corrections), and frequency of standards run and standardization approaches. Different labs have variable measurement procedures, with a range of integration times (less than 400 seconds - to 1200 seconds or more), sample sizes (sub-mg or larger for a single analysis), and replication (3 or less to >8). Standard corrections differ, with some labs averaging standard values over multiple days or weeks for corrections, while other labs characterize short-term drift. Some datasets necessitated the use of transfer functions to convert from CDES to I-CDES reference frames (Tripati et al., 2010; Breitenbach et al., 2018; Peral et al., 2018), which uses average standard δ^{47} values. However, this should contribute < 3 ppm for δ^{47} values within ± 18 ‰ of ETH-1 (Bernasconi et al., 2021).

These foraminiferal calibration data come from six clumped isotope laboratories (Table 1) that utilize different instruments and analytical methods. There is particularly strong agreement between data from Tripati et al. (2010), Breitenbach et al. (2018), Meinicke et al. (2020), and this study (Eagle-Tripati lab), that overlap with each other including at the extremes of the highest and lowest temperatures. All of these datasets show more variability at warmer temperatures, which could reflect the larger sample density relative to cold regions.

Each dataset included in this study has regression slopes and intercepts that fall within the 95% confidence intervals of each other (Supporting Information Table S6). Within the foraminiferal data synthesis for 260 samples, dataset-related (i.e., methodological artifacts) account for up to 11% of the variance from our non-thermal R-model based effect size testing. This largely comes from two datasets that are amongst the three smallest in terms of sample numbers (Peral et al., 2018 - 27 samples; Piasecki et al., 2019 - 13 samples). The relatively small sample sizes could potentially explain these offsets, although we cannot preclude that differences in instrumentation and/or standardization during the specific intervals that samples were run may also be a contributing factor. At low temperatures, both the Peral et al. (2018) and reprocessed Peral et al. (2022) results are offset from the other studies, with a slightly steeper slope, while the Piasecki et al. (2019) benthic foraminiferal values are positively offset from other studies, especially at higher temperatures, and exhibit a shallower slope (Supporting Information Table S6).

3.3.2 Biological

3.3.2.1 Ecology

Here, if we subdivide benthic foraminiferal data by habitat (Figures 3 and 4), we see that the slopes and intercepts of both the infaunal and epifaunal species individually fall within the 95% confidence intervals of planktic regression slope and intercept. While the mixed benthic species regression does not overlap with the planktic regression 95% CI, this is likely a result of low data density at warmer temperature, an artifact of how measurements were combined between species (e.g., Piasecki et al., 2019), potential mixing effects, or a combination of these factors. It is also possible that some of the data are offset due to other potential non-thermal effects that the benthic population is sampling (e.g., a carbonate ion saturation effect, discussed further below).

3.3.2.2 Taxon-specificity

Temperature proxies including foraminiferal $\delta^{18}O$ and Mg/Ca show that interspecific offsets exist for multiple taxa (e.g., Bemis et al., 1998; Jentzen et al., 2018; Marchitto et al., 2014; Regenberg et al., 2009). Previous studies looking for such effects in Δ_{47} have suggested that there are little to no vital effects on this thermometer (Tripati et al., 2010; Grauel et al., 2013; Peral et al., 2018; Meinicke et al., 2020, Daëron and Gray, 2023). However, this previous work on Δ_{47} has investigated relatively small numbers of species, with limited numbers of localities sampled for each species (typically n < 7). Here, with our new data and the meta-analysis, we assess taxon-specific effects using data for 29 species, with n>20 for five species.

Our analysis indicates that taxon-specific offsets are not resolvable when subgroups of data are examined (Figure 5). If grouped by genus, mean residuals (Δ_{47} observed minus Δ_{47} predicted from the calibration for all foraminifera) for 14 taxa are smaller than +/-0.005 ‰, and for all but one taxa are less than +/-0.01 ‰. At the genus level, residuals are indistinguishable from a normal distribution at the 95% confidence level for 10 out of 12 genera, the exceptions being *Trilobatus* and *Uvigerina* where there is a skewness of -0.10 and -2.03 respectively. The skew in the data for *Uvigerina* (n = 9) is driven by a single point that lies far outside the rest of the samples. *Trilobatus* comprises two species and when these are looked at individually, each species is not distinguishable from a normal distribution at the 95% confidence level (*T. sacculifer:* W = 0.94203831, p = 0.09396572; *T. trilobus:* W = 0.97780615, p = 0.88903859), but when combined reflect a larger trend in the overall dataset of a minor skew to the left (Figure S9).

If considered at the species-level, mean species residuals for 17 taxa are smaller than +/-0.005 ‰, and for all but 5 taxa are less than 0.01 ‰. Residuals are indistinguishable from a normal distribution other than *N. pachyderma* (Shapiro-Wilk test, p > 0.05). For the five species represented at a large number of localities (*P. obliquiloculata, T. sacculifer, G. tumida, G. bulloides, G. ruber)*, mean residuals are less than 0.005 ‰ (Figure 5, S9). All but one species exhibit residuals within +/-0.02 ‰, which is the long-term standard deviation for standards reported for different instruments and by multiple labs (e.g., Meckler et al., 2014; Bernasconi et al., 2021; Upadhyay et al., 2021). These residuals are normally distributed for all taxa that have a large number of samples.

Figure 4: Regressions through subsets of core-top foraminiferal data and foraminiferal compilation. All subsets are plotted on top of the foraminiferal compilation (grey) with subsets highlighted as follows: a) Planktic foraminifera b) Benthic foraminifera c) Mixed-layer planktics d) Mixed benthics e) Infaunal benthics f) Epifaunal benthics. 95% confidence interval is also shown.

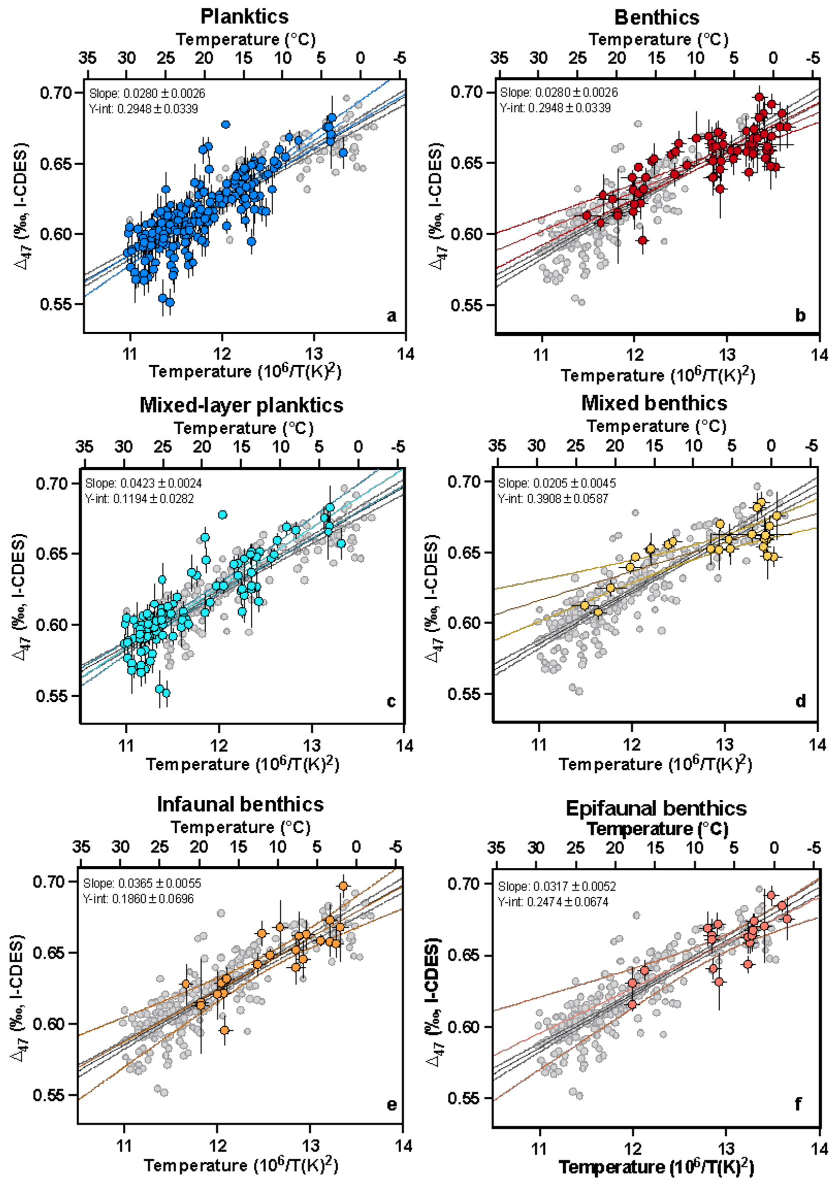

We note that the taxa with larger residuals and non-normal distributions could bias the regression, and thus, we assessed impacts of individual species on the slope and intercept of the overall calibration line by removing species individually from the calculation and reporting the resulting values, following the approach of Meinecke et al. (2020). When using this approach, both slopes and intercepts still remain well within error of the primary regression, suggesting that individual taxa are not unduly influencing the regression (Supporting Information Table S6).

We investigated other potential biological effects on Δ_{47} associated with mineralogy and photosymbionts. *H. elegans* is an aragonitic species of foraminifera and was measured in multiple studies. However, we do not observe any systematic offsets of data from this species (Figure 5, Supporting Information Table S6). Photosymbiosis in foraminifera affects both calcification rates and microenvironments (de Nooijer et al., 2014) and has the potential to cause disequilibrium isotopic values (e.g., Spero et al., 1997). We do not observe systematic offsets when comparing non-photosymbiont bearing species and photosymbiont bearing species at the 95% confidence interval (Figure S10).

Figure 5: Δ_{47} residuals for different taxa calculated as $\Delta_{47observed}$ minus $\Delta_{47calculated}$ using the foraminiferal calibration equation from our meta-analysis. a) Species-specific residuals. b) Grouped genus residuals.

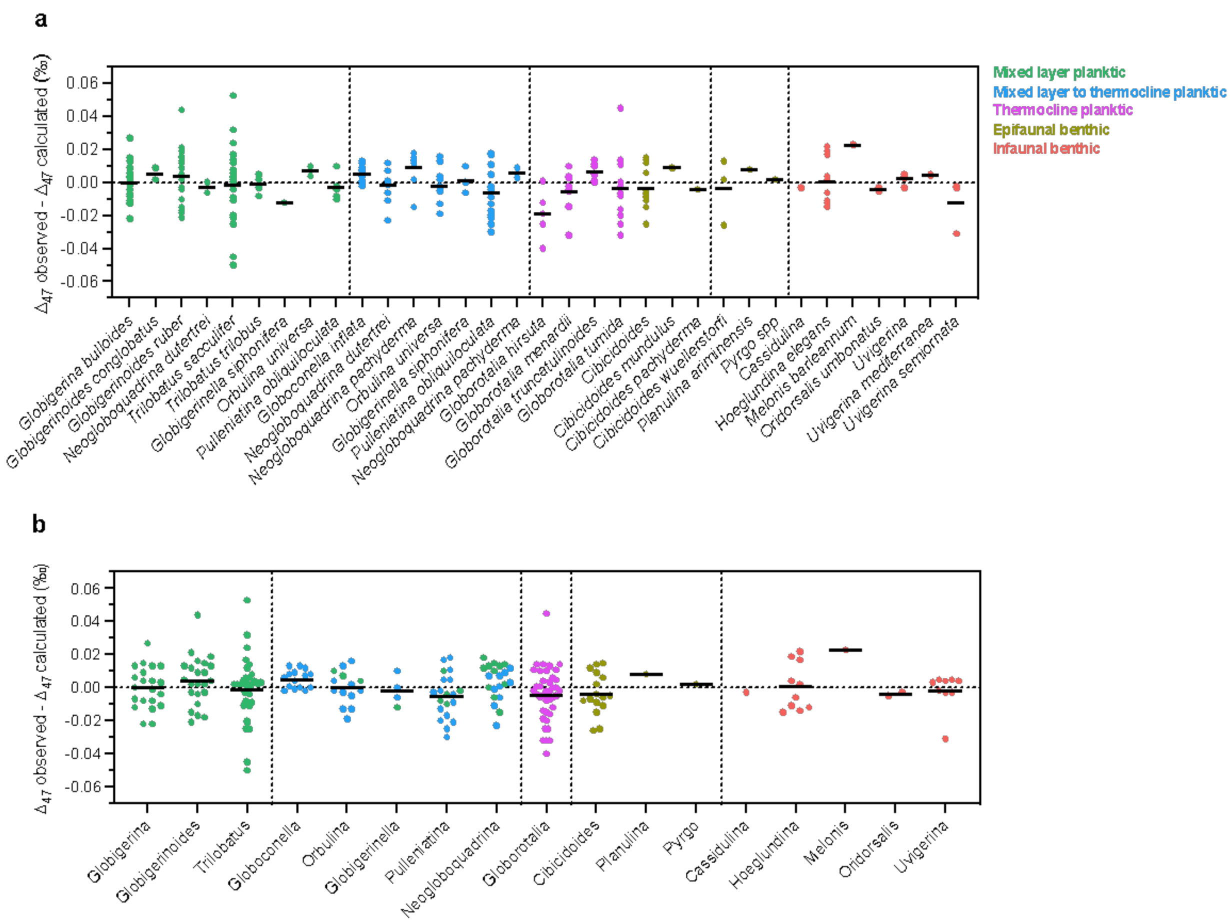

3.3.2.3 Oceanic region

Given basin-specific Mg/Ca calibrations (e.g., Skinner et al., 2007) and region-specific genotypes (Sadekov et al., 2016; Darling et al., 2017), we explored whether geography impacted calibration in the meta-analysis. For all regions with large numbers of samples (Atlantic Ocean, Pacific Ocean, Indian Ocean, Gulf of Mexico), 95% confidence intervals overlapped with the broader foraminiferal calibration (Figure S11). The Arctic Ocean contains only a small number of samples and a limited temperature range so the uncertainties in a basinal calibration are large, and additional calibration material from this region (and other high latitude areas) are critical.

3.3.3 Seawater Chemistry

Given evidence for seawater chemistry impacts on Mg/Ca, we explore if there are discernable effects of seawater chemistry on Δ_{47} in foraminifera. We first used PCA to assess how much variance in hydrographic parameters as potential predictors can be attributed to different factors, and whether any potential model components are strongly correlated with one another. We find no evidence of such correlations between hydrographic parameters, when investigating temperature, salinity, carbonate saturation, and depth (Figure S12). Below, we describe the relationship between Δ_{47} residuals and salinity. We also examine if in benthic foraminifera, Δ_{47} is correlated with saturation state.

3.3.3.1 Salinity

Salinity variation has been shown to affect Mg/Ca sensitivity by around 4.5 % per salinity unit depending on the species (e.g., Ferguson et al., 2008; Hönisch et al., 2013). A small salinity effect on Δ_{47} associated with the salinity-dependence of dissolved inorganic carbon (DIC) speciation has been predicted from theory, but was not thought to be impactful over the salinity range of the oceans (Tripati et al., 2015). Consistent with this prediction, previous studies on clumped isotopes in foraminifera that had small sample sizes suggest no detectable correlation with salinity (Grauel et al., 2013; Peral et al., 2018).

We examined the larger dataset to see if a salinity effect was detectable. Foraminifera from this study cover a salinity range of 33.0 to 38.8 PSU and as a whole similarly show no clear correlation of salinity with Δ_{47} residuals (Pearson's correlation p-value = 0.77, Figure S13). These results support theoretical predictions (Tripati et al., 2015). However, Pearson's correlation between the two variables has a p-value of 0.01 for the benthic data. This correlation does not appear in the planktic data. Analysis of the correlation between temperature and salinity ranges in the benthic data suggest that the correlation observed may be due to offsets in temperature trends observed in section 3.2.2 rather than a true salinity effect (Figure S13).

3.3.3.2 Carbonate saturation effects on benthics

Seawater carbonate chemistry has been shown to impact benthic foraminiferal Mg/Ca (Elderfield et al., 2006). A number of approaches have been used to detect such an effect, including direct comparisons of benthic Mg/Ca to seawater $\Delta[CO_3^{2-}]$, a comparison of temperature-corrected Mg/Ca to $\Delta[CO_3^{2-}]$, as well as the use of a multiple linear regression to examine the sensitivity to temperature and carbonate ion (Elderfield et al., 2006). Based on culturing studies, a carbonate ion effect in $\delta^{18}O$ has been observed in planktic foraminiferal calcite and coral aragonite (Spero et al., 1997). In benthic foraminifera, disequilibrium in $\delta^{18}O$ can systematically vary between taxa, linked to carbonate ion (Bemis et al., 1998; Ishimura et al., 2012; Rathman and Kuhnert, 2008). For $\delta^{18}O$, this disequilibrium is hypothesized to be related to changes in the isotope composition of the dissolved inorganic carbon pool as a function of pH (Zeebe, 1999).

When we compare benthic Δ_{47} residuals ($\Delta_{47observed}$ minus $\Delta_{47calculated}$ using the foraminiferal temperature calibration equation from our meta-analysis) to $\Delta[CO_3^{2-}]$ (Figure 6), we find a significant positive correlation, consistent with a weak sensitivity of benthic Δ_{47} to changing carbonate ion (Figure 6B; slope = 0.00019, R^2 = 0.315, p <0.01). We note that the correlation largely reflects a significant relationship in the epifaunal benthic foraminiferal data significant at the >95% confidence level (Figure 6C; slope = 0.00018, R^2 = 0.315, p = 0.043, n = 19), and in the mixed benthics data (Figure 6E; slope = 0.00022, R^2 = 0.482, p <0.01, n = 24). The data showing this trend were generated as part of this study and by Piasecki et al. (2019) (Figure 6A). No significant correlation is found at the >95% confidence level in the infaunal benthic data (Figure 6D).

If we directly compare benthic Δ_{47} to $\Delta[CO_3^{2-}]$, a significant but weak (p=0.01, R^2=0.09) is observed in the meta-analysis (Figure S14). This pattern is similar to what was reported for benthic Mg/Ca (Elderfield et al., 2006). However, different sub-groups of the benthic foraminiferal data (e.g., epifaunal benthics, infaunal benthics, etc.) do not exhibit significant linear correlations, but this may not be surprising if an effect is present but relatively weak.

We developed benthic multivariable regressions that account for a dependence of Δ_{47} on both temperature and $\Delta[CO_3^{2}]$, in the form of Δ_{47} (‰) = $\beta 0 + \beta 1 \times 10^6/\text{Temperature (K)}^2 + \beta 2 \times \Delta[CO_3^{2-}]$ (Table 4 and Figure 7). These analyses also support sensitivities of Δ_{47} to $\Delta[CO_3^{2-}]$ that are generally similar in magnitude to those derived using other methods (e.g., regressing Δ_{47} residuals against $\Delta[CO_3^{2-}]$), with values of 0.0017 for all benthic foraminifera, 0.0015 for all benthic foraminifera (epifaunal and infaunal benthics), 0.0019 for epifaunal benthic foraminifera, and 0.0013 for infaunal benthic foraminifera (Figure 7, Table 4).

Figure 6: Benthic Δ_{47} residuals vs. $\Delta[CO_3^{2-}]$. Residuals calculated as $\Delta_{47observed}$ minus $\Delta_{47calculated}$ using the foraminiferal calibration equation from our meta-analysis. a) Benthics separated by study, b) all benthics, c) epifaunal benthics, d) infaunal benthics, e) mixed benthics, f) all benthics (infaunal + epifaunal).

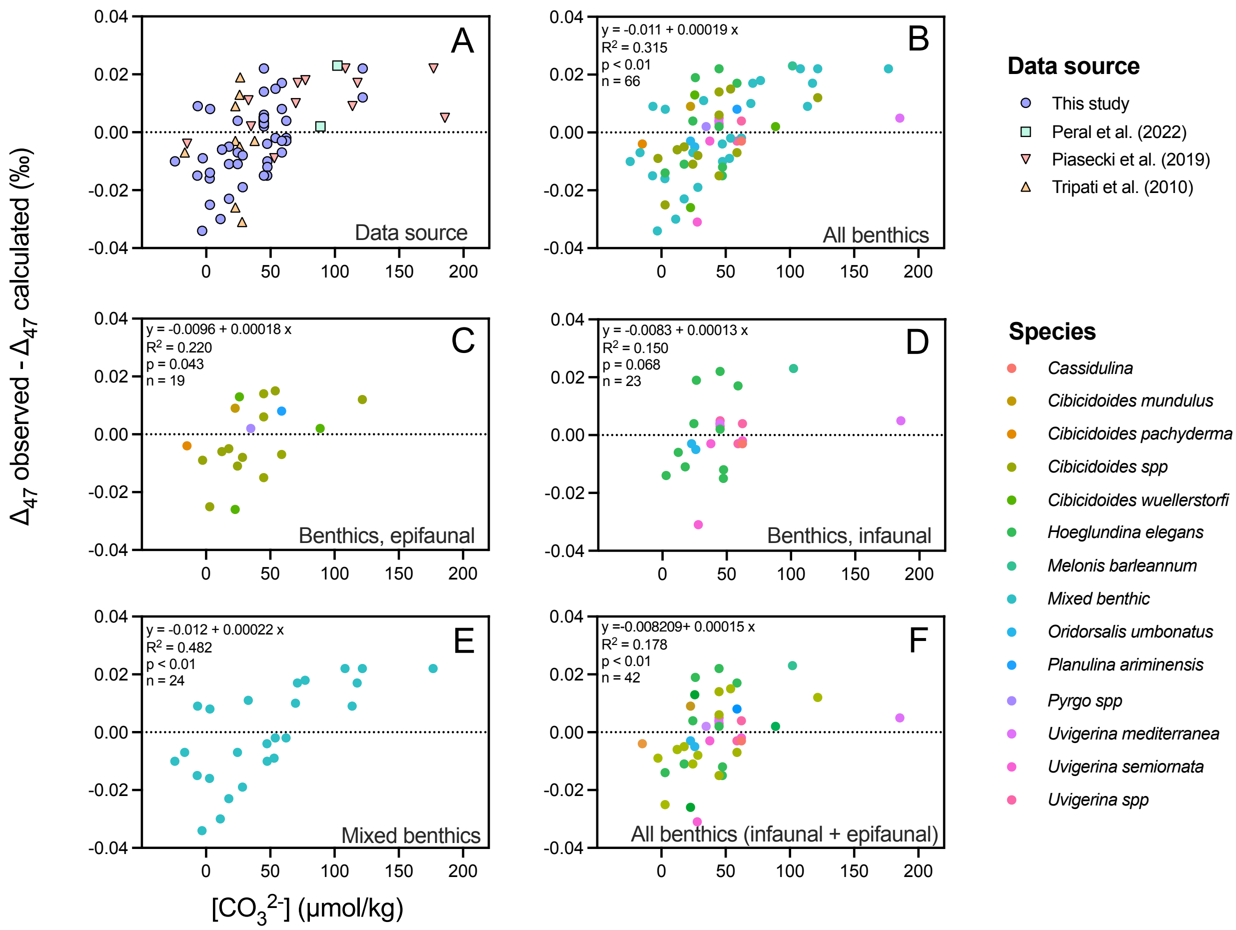

3.3.4 R-based model selection

3.3.4.1 Evaluation of non-thermal effects in UCLA dataset

The benthic foraminiferal dataset from the Eagle-Tripati lab at UCLA (n = 42) is best explained by a model with temperature as the sole predictor ($F_{1,40} = 64.6$, SE = 0.01, Adjusted $R^2 = 0.608$, $p < 0.00001$; Supporting Information Table S7). If planktic foraminiferal Δ_{47} from the UCLA dataset is considered, the signal is best explained by an additive model containing temperature, bottom water carbonate saturation (i.e., a dissolution effect), and photosymbiont presence/absence ($F_{3,78} = 50.9$, SE = 0.01, Adjusted $R^2 = 0.649$, $p < 0.00001$; Supporting Information Table S7). Temperature explains the vast majority of the variation in Δ_{47} (Partial $\eta^2 = 0.57$, lower 95% CI 0.46; Supporting Information Table S7), followed by bottom water carbonate saturation and photosymbiont presence/absence, which both have a "medium" effect, and return the same effect size and lower 95% CI (Partial $\eta^2 = 0.06$, lower 95% CI 0.0). Temperature has a large positive effect of 0.029 ± 0.003 ‰ on Δ_{47} for each 1 σ increase. Bottom water carbonate saturation in the linear model exhibits a slight positive effect of 0.006 ± 0.003 ‰ on Δ_{47} per 1 σ increase in carbonate ion saturation. Photosymbiont presence produces a slight positive offset in Δ_{47} relative to taxa who lack photosymbionts of 0.009 ± 0.004 ‰.

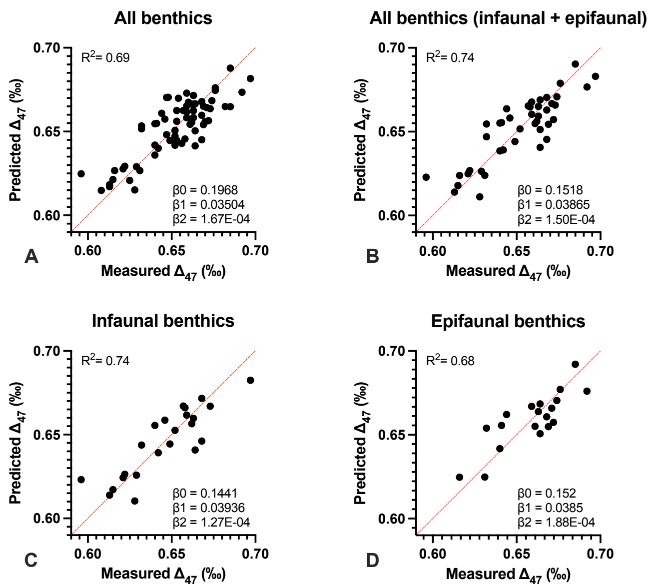

Figure 7: Predicted Δ_{47} compared to measured Δ_{47} for benthics. Predicted Δ_{47} is from a multivariate regression of the form Δ_{47} (‰) = β0 + β1 x $10^6/T^2$ + β2 x $\Delta[CO_3^{2-}]$ (regression parameters in Table 4). a) all benthics, b) all benthics (infaunal + epifaunal), c) infaunal benthics, and d) epifaunal benthics. There are at least two different ways, in theory, that Δ_{47} could be affected by bottom water carbonate saturation. First, a small effect has been predicted from theory and observed in experiments for Δ_{47}, with a difference in the equilibrium isotopic composition of DIC species at pH between 7 and 11 of ~0.03 to 0.05 ‰, that was predicted to give rise to effects of less than 0.02 ‰ for the Cenozoic, and lower Δ_{47} at elevated pH (Hill et al., 2014; Tripati et al., 2015). A second effect, with increasing Δ_{47} associated with increased pH, could arise from a possible CO_2 hydrolysis effect that increases with precipitation rate (Guo, 2020; Lucarelli et al., 2022; Tripati et al., 2015). Experimental studies have observed this effect only at low temperature and elevated pH (pH > 9.5) with decreased effect size in the presence of carbonic anhydrase recently shown to be active in some benthic foraminiferal species (de Goeyse et al., 2021; Lucarelli et al., 2022).

3.3.4.2 Statistical model investigation of non-thermal effects in meta-analysis of benthic and planktic foraminifera

Benthic foraminiferal Δ_{47} in the meta-analysis (n = 67) is best explained by the additive effects of temperature, bottom water carbonate saturation, and salinity ($F_{3,63}$ = 54.4, SE = 0.01, Adjusted R^2 = 0.708, p <0.00001). Temperature again explains the vast majority of the variation in Δ_{47} (Partial η^2 = 0.60, lower 95% CI 0.47; Supporting Information Table S7), followed by carbonate saturation (Partial η^2 = 0.25, lower 95% CI 0.11), and salinity (Partial η^2 = 0.08, lower 95% CI 0.01). Temperature has a positive effect on Δ_{47} of 0.022 ± 0.002 ‰ for each 1 σ increase; carbonate saturation has a slight positive effect of 0.009 ± 0.002 ‰; and salinity has a slight negative effect of 0.005 ± 0.002 ‰. We found no evidence of a significant effect of benthic foraminiferal habitat (epifaunal versus infaunal) on the final Δ_{47} signal (Estimate = -0.0001, Std err = 0.004, t = -0.033, p = 0.97).

For the meta-analysis, planktic foraminiferal Δ_{47} (n = 193) is explained by multiple variables. Model selection identified three-way interactions between temperature, dataset, and bottom water carbonate saturation; and temperature, bottom water carbonate saturation (i.e., dissolution), and photosymbiont presence/absence ($F_{23,169}$ = 31.6, SE = 0.01, Adjusted R^2 = 0.786, p <0.00001). Temperature explains the vast majority of the variation in Δ_{47} (Partial η^2 = 0.62, lower 95% CI 0.55; Supporting Information Table S6), followed by the interaction between dataset and bottom water carbonate saturation (Partial η2 = 0.21, lower 95% CI 0.11); dataset alone and the three-way interaction between temperature, dataset, and carbonate saturation (Partial η2 = 0.15, lower 95% CI 0.07); (Both: Partial η^2 = 0.14, lower 95% CI 0.06); carbonate saturation alone (Partial η2 = 0.10, lower 95% CI 0.04) and the two-way interaction between temperature and carbonate saturation (Partial η^2 = 0.06, lower 95% CI 0.01), with all other combinations having an effect size of 0.04 or less.

Table 4: Multivariable regressions between Δ_{47} (‰), temperature T (K) and $\Delta[CO_3^{2-}]$ (µmol/kg).

Δ_{47} (‰) = β0 + β1 x $10^6/T^2$ + β2 x $\Delta[CO_3^{2-}]$						
All benthics						
Parameter estimates	Variable	Estimate	Standard error	P value	R^2	n
β0	Intercept	0.1968	0.0415	<0.0001	0.6926	67
β1	$10^6/T^2$	0.03504	0.003138	<0.0001		
β2	$\Delta[CO_3^{2-}]$	0.0001673	0.00004572	0.001		
All benthics (epifaunal and infaunal benthics)						
Parameter estimates	Variable	Estimate	Standard error	P value	R^2	n
β0	Intercept	0.1518	0.04932	0.0038	0.7427	42
β1	$10^6/T^2$	0.03865	0.00376	<0.0001		
β2	$\Delta[CO_3^{2-}]$	0.0001495	0.00006014	0.0173		
All infaunal benthics						
Parameter estimates	Variable	Estimate	Standard error	P value	R^2	n
β0	Intercept	0.1441	0.06748	0.0453	0.743	23
β1	Temperature	0.03936	0.005239	<0.0001		
β2	$\Delta[CO_3^{2-}]$	0.0001271	0.00007825	0.1199		
All epifaunal benthics						
Parameter estimates	Variable	Estimate	Standard error	P value	R^2	n
β0	Intercept	0.152	0.09113	0.1147	0.6838	19
β1	Temperature	0.03851	0.006841	<0.0001		
β2	$\Delta[CO_3^{2-}]$	0.000188	0.0001059	0.0949		

3.3.4.3 Statistical model investigation of non-thermal effects in full foraminiferal dataset

R-based model selection indicates that temperature effects vastly outweigh non-thermal signals in the full foraminiferal dataset (n = 260) (Supporting Information Table S6). Non-thermal effects can account for up to 13% of the variance in the dataset if all other variables are held constant. Foraminiferal Δ_{47} is best explained by temperature, plus the effects of three two-way interactions (foraminiferal type and bottom water carbonate saturation; dataset and depth; dataset and photosymbiont presence/absence; $F_{20,239}$ = 60.8, SE = 0.01, Adjusted R^2 = 0.822, p <0.00001; Supporting Information Table S6). Temperature has a positive effect on Δ_{47} of 0.028 ± 0.001 ‰ for each 1 σ increase. The interaction between dataset and depth accounts for 13% of the variance (Partial η^2 = 0.13, lower 95% CI 0.06, followed by dataset alone, which accounts for 10% of the variance in Δ_{47} (Partial η^2 = 0.10, lower 95% CI 0.03). All other model terms have a partial η^2 of 0.05 or less.

3.4 Vertical profiles of temperature reconstructed from core-top planktics

We assess the utility of using foraminiferal Δ_{47}-derived temperature estimates in reconstructing oceanic water column thermal properties in different oceanographic regions. For planktics, Δ_{47}-temperature estimates are calculated using the full foraminiferal regression from the meta-analysis. We compared WOA temperature profiles with Δ_{47}-reconstructed temperatures from multiple species we analyzed from the Arctic Ocean, North Atlantic, Indian Ocean, and Western Equatorial Pacific (Figure 8; Figures S15-S17). Reconstructed temperatures are plotted at assumed calcification depths for each taxa at each site (Figure 8, Supporting Information Table S2). A cross comparison of Δ_{47}-temperature and expected temperature based on calcification depth shows good agreement (slope of 0.99 ± 0.03, $R^2 = 0.75$ and $p < 0.001$).

Figure 8: Reconstructed Δ_{47}-temperatures a) Comparison of Δ_{47}-temperature with $\delta^{18}O$-based calcification temperatures (method 2) for all core-top samples. Linear regression has a slope of 0.99 ± 0.03, $R^2 = 0.75$ and $p < 0.001$ ($n = 260$). Reconstructed temperature profiles based on clumped isotopes temperature for b) the Indian Ocean, c) Western Pacific, d) North Atlantic and e) Arctic Ocean.

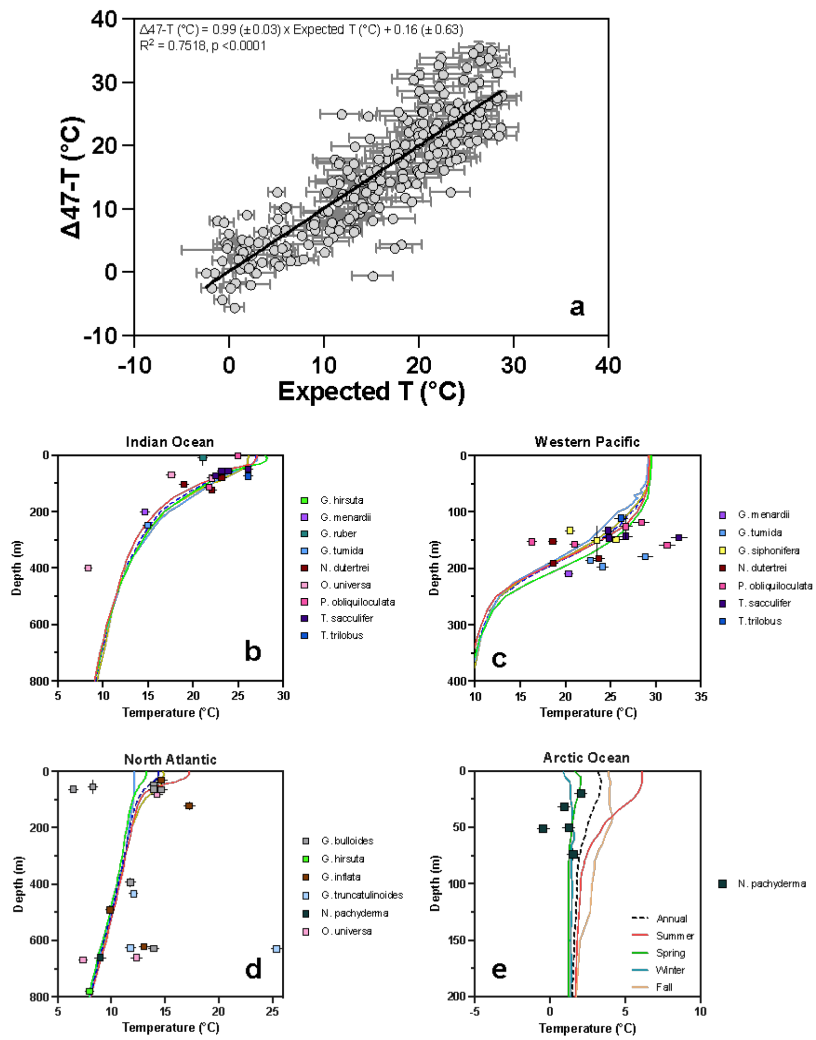

Most Δ_{47}-temperatures plot within error of measured water temperature profiles. With the exception of the Arctic data, there is little indication of seasonality being resolvable using this method because typically, the uncertainty in Δ_{47}-temperatures is greater than the seasonal extremes of temperatures at the sites chosen. Interestingly, in the case of near freezing temperatures, our results show no systematic offset from the measured site temperatures which suggests that there is no observed isotopic offset introduced by calcification at these cold temperatures in foraminifera suggested in other studies (Tripati et al., 2010), although it should be noted that samples in this region are limited only to the species *N. pachyderma*.

3.5 Recalculating Cenozoic bottom water temperatures using new calibrations

Daeron and Gray (2023) and Rohling et al. (2024) discuss some of the differences between published reconstructions of bottom water temperatures from benthic foraminiferal Δ_{47} and $\delta^{18}O$, including discrepancies between proxy predictions for the Late Paleocene, Eocene, Eocene-Oligocene transition, and Pleistocene, highlighting the importance of utilizing new calibration data and constraints from carbonate chemistry in such calculations. Thus, here we apply the new calibrations to benthic foraminiferal data and evaluate Δ_{47}-temperatures and seawater water $\delta^{18}O$. We recalculate Cenozoic temperatures with low-resolution benthic Δ_{47}-data from Meckler et al. (2022) for the North Atlantic from IODP Expedition 342 (Sites 1406, 1407, 1409, and 1410) on the CENOGRID timescale (Westerhold et al., 2020). We recalculate Eocene-Oligocene temperatures using benthic Δ_{47}-data from Taylor et al. (2023) for ODP Site 1218 and IODP Sites U1333 and U1334 from the Pacific and the ages reported therein.

Below, we discuss results from the different calibration approaches for the Pleistocene (Section 3.5.1), Eocene-Oligocene transition (Section 3.5.2), Early Eocene Climatic Optimum (Section 3.5.3), and Paleocene (Section 3.5.4). We also calculate the potential scope of impacts on benthic reconstructions for the PETM (Section 3.5.5). In each section, we compare the originally published benthic Δ_{47}-reconstructions that utilize the planktic calibration of Meinicke et al. (2020) to values calculated using (1) the new Δ_{47}-temperature calibrations and (2) the new benthic multivariate Δ_{47} calibration that also factor changes in carbonate chemistry into estimates of temperature and seawater $\delta^{18}O$ (Supporting Information Table S8-10). For the latter, to constrain changes in carbonate chemistry, one can use site- or region-specific estimates of bottom water carbonate saturation based on Li/Ca or B/Ca data from benthic foraminifera (Lear and Rosenthal, 2006, Yu et al., 2007), which is the approach we use in Section 3.5.2 (the Eocene-Oligocene transition) because Li/Ca data were available. Another approach that may be less accurate is to utilize a combination of constraints on two different carbonate system parameters using proxy and/or carbon cycle model calculations (e.g., Meckler et al., 2022; Roberts and Tripati, 2009; Tyrell and Zeebe, 2004). This first-order calculation of the impact of $[CO_3^{2-}]$ on Δ_{47}-temperatures is what we utilize for the other sections. We calculated $[CO_3^{2-}]_{in\ situ}$ using CO_2sys excel (v. 2.3. Pierrot et al. 2016) and published constraints on pCO_2 and Total alkalinity (Supporting Information Table S8). pCO_2 was interpolated from a 50 points average record from Hönisch et al. (2023) based phytoplankton and boron isotopes. Total alkalinity was interpolated using the published record from Tyrell and Zeebe (2004). The precipitation constant for calcite (Ksp, Mucci et al. 1983) was calculated using a constant salinity of 35 and the published temperature from clumped isotopes. $[CO_3^{2-}]_{sat}$ was then determined for Ω=1 and $[Ca^{2+}]$ interpolated from Horita et al. (2002).

3.5.1 Cooler Pleistocene temperatures calculated using new benthic Δ_{47}-temperature calibrations

Pleistocene temperatures estimated by Meckler et al. (2022) range from -0.3 °C to 3.4 °C, and average 1.6 °C (Figure 9, Supporting Information Table S9). All of the new Δ_{47}-temperature calibrations yield cooler estimates of Pleistocene temperatures (Figure 9, Supporting Information Table S9). For example, the “all foraminifera-MB” regression gives similar values to the temperature calibration from Anderson et al. (2021) for the Pleistocene, with Δ_{47}-temperatures ranging from -1.8 to 1.6 °C for the “all foraminifera-MB” and -1.5 to 1.9 °C using the Anderson et al. (2021) regression. Temperatures calculated using the “all benthics” calibration range from -5.1 to 0.5 °C and the “infaunal” regression from -2.3 to 1.3 °C. The “all benthics (infaunal + epifaunal” and “epifaunal” regressions yield similar results to each other for the Pleistocene, with temperatures ranging from -3.1 to 0.6 °C for “all benthic – MB” and from -3.8 to 0.3 °C for “epifaunal”. The full foraminifera calibration supports temperatures in between -2.2 to 1.3 °C.

Estimates of $\delta^{18}O_{sw}$ from these calibrations are lower than those estimated from Meckler et al. (2022), with values of 0.44 ‰ for the “all foraminifera - MB” calibration, 0.71 ‰ for the “All benthic (infaunal + epifaunal)” regression, 0.85 ‰ for the “epifaunal” regression, and 0.54 ‰ for the “infaunal” regression (Figure 9, Supporting Information Table S9). For the “compiled benthic”, “All benthic (infaunal

+ epifaunal)", and "epifaunal" regressions, the average $\delta^{18}O_{sw}$ is negative (Figure 9, Supporting Information Table S9). Note that negative $\delta^{18}O_{sw}$ values for the Pleistocene are not likely given that average global ice-volumes are expected to be between interglacial and glacial extremes, which should lead to positive $\delta^{18}O_{sw}$ values (Cramer et al., 2011).

3.5.1.1 Pleistocene temperatures from the new benthic multivariate Δ_4-calibration

Figure 11 shows Pleistocene values of temperature that are calculated using the "All benthic (infaunal + epifaunal)" multivariate calibration. Pleistocene Δ_{47}-temperatures for the Atlantic range from -0.7 °C to 3.0 °C, in better agreement with the temperature estimates from Meckler et al. (2022) (Figure 11, Supporting Information Table S8). Estimates of $\delta^{18}O_{sw}$ range from -0.09 to 1.14 ‰ and average 0.55 ‰. The positive $\delta^{18}O_{sw}$ predicted by the multivariate regression is in better agreement with estimates of ice volumes from the Pleistocene (Cramer et al., 2011).

3.5.2 Cooler Eocene-Oligocene bottom water temperatures from the new benthic Δ_{47}-temperature calibrations

We recalculate tropical Pacific Ocean bottom water temperatures using benthic Δ_{47} data from Taylor et al. (2023) (that used the planktic calibration of Meinicke et al., 2020) for ODP Site 1218 and IODP Sites U1333 and U1334. These sites were located at a paleodepth of 3500 to 4000 m. This transition is associated with the permanent establishment of large ice sheets on Antarctica and a ~1 km deepening of carbonate compensation depth in the Pacific Ocean (Coxall et al., 2005). It is thought that the deepening of the carbonate compensation depth was global (Tripati et al., 2005) and associated with a rise in $[CO_3^{2-}]$ (Pusz et al., 2011). Taylor et al. (2023) report late Eocene Δ_{47}-temperatures of 11.0 °C and Earliest Oligocene temperatures of 9.7 °C, with a change across the Early Oligocene Oxygen Isotope Step (EOIS, absolute temperature of 6.5 °C) of -4.7 ± 0.9 °C.

We apply the new foraminiferal Δ_{47}-temperature calibrations, with recalculated values shown in Supporting Information Tables S9-10 and Figure 9. Overall, all of the new (non-multivariate) benthic Δ_{47}-T calibrations result in absolute temperatures that are cooler by ~2-2.5 °C, compared to what was originally reported by Taylor et al. (2023) using the planktic calibration of Meinicke et al. (2020). The amplitude of changes in temperature and $\delta^{18}O_{sw}$ are slightly larger or similar to what was published by Taylor et al. (2023).

3.5.2.1 Lower $\delta^{18}O_{sw}$ values using the new benthic Δ_{47}-temperature calibrations

The Taylor et al. (2023) estimates of late Eocene $\delta^{18}O_{sw}$ are 0.35 ‰ to 0.89 ‰ for the early Oligocene. They report an increase of $\delta^{18}O$ seawater of 0.07 ‰ over EOIS and a change of 0.54 ‰ across the transition. As reference, a change of 0.6 ‰ across the transition is estimated to lead to a change of ice volume on the order of 70 %–110 % relative to modern. The new benthic Δ_{47}-temperature calibrations yield absolute $\delta^{18}O_{sw}$ values are ~0.4 to 0.6 ‰ lower, and the changes in $\delta^{18}O_{sw}$ are slightly larger or similar to what was published (Supporting Information Table S9).

A puzzling pattern emerges when looking at calculated changes in $\delta^{18}O_{sw}$ in more detail, specifically if we look at the values of $\delta^{18}O_{sw}$ associated with the EOIS from the different calibrations. We would expect a positive change in $\delta^{18}O_{sw}$ associated with the oxygen isotope step, given the growth of ice, yet some of the new regressions, from "all benthic-MB", "all benthic", "infaunal" and "epifaunal", yield negative changes in $\delta^{18}O_{sw}$ associated with the EOIS, although they do give positive changes across the broader EOT. For example, the "all benthic-MB" calibration gives late Eocene mean temperatures of 9.3 °C, a temperature change associated with the EOIS of -4.6 °C and an associated $\delta^{18}O_{sw}$ change of 0.04 ‰, and a change across the EOT of 0.53 ‰ (Supporting Information Table S9). The "epifaunal" calibration yields 9.6 °C, with a -5.5 °C change and a -0.18 ‰ $\delta^{18}O_{sw}$ change across the EOIS, and a 0.47 ‰ change across the transition.

3.5.2.2 Reasonable Δ_{47}-T and $\delta^{18}O_{sw}$ values from the new benthic multivariate Δ_{47}-calibration

The most robust absolute values and patterns of change in temperature and $\delta^{18}O_{sw}$ are reconstructed using the All benthic (infaunal + epifaunal) multivariate equation. To apply the multivariate calibration, we utilize a series of constraints. Estimates of the increase in $[CO_3^{2-}]$ derived from Li/Ca ratios in benthic foraminifera associated with the Oi-1 glaciation range from ~36 µmol/kg at ODP Site 1218 in the equatorial Pacific Ocean (Lear et al., 2010; Lear and Rosenthal, 2006) to ~29 µmol/kg at ODP Site 1263 in the South Atlantic on Walvis Ridge (Peck et al., 2010). Modern carbonate profiles in this region have a bottom water $[CO_3^{2-}]$ = 81 µmol/kg (GLODAP database corrected from anthropogenic inputs, modern profiles), $[CO_3^{2-}]_{sat}$ = 87 µmol/kg, and a $\Delta[CO_3^{2-}]$ = -6 µmol/kg. If we apply the estimated change in $[CO_3^{2-}]$ from ODP Site 1218 across the Eocene-Oligocene Transition, we calculate a $\Delta[CO_3^{2-}]$ from -6 to 30 µmol/kg.

Figure 9: Reconstructed Δ_{47}-based estimates of bottom water temperatures and $\delta^{18}O_{sw}$ for the Eocene-Oligocene Transition. Temperatures are cooler for all of the new regressions from this study (colored lines), and most $\delta^{18}O_{sw}$ values lower, compared to Taylor et al. (2023) (grey line). The multivariate regression shows the largest $\delta^{18}O_{sw}$ increase across the EOT. Light blue and pink lines show Δ_{47}-temperatures based on the all benthic (infaunal + epifaunal) multivariate equation at different $\Delta[CO_3^{2-}]$. The dashed line combines these lines to correct for $\Delta[CO_3^{2-}]$ across the event. The dark blue line shows the non-multivariate Δ_{47}-temperatures with no correction for $\Delta[CO_3^{2-}]$. The grey line shows original reconstruction from Taylor et al. (2023) that used planktic calibration from Meinicke et al. (2020) for comparison. All calculations use Δ_{47} data from Taylor et al. (2023).

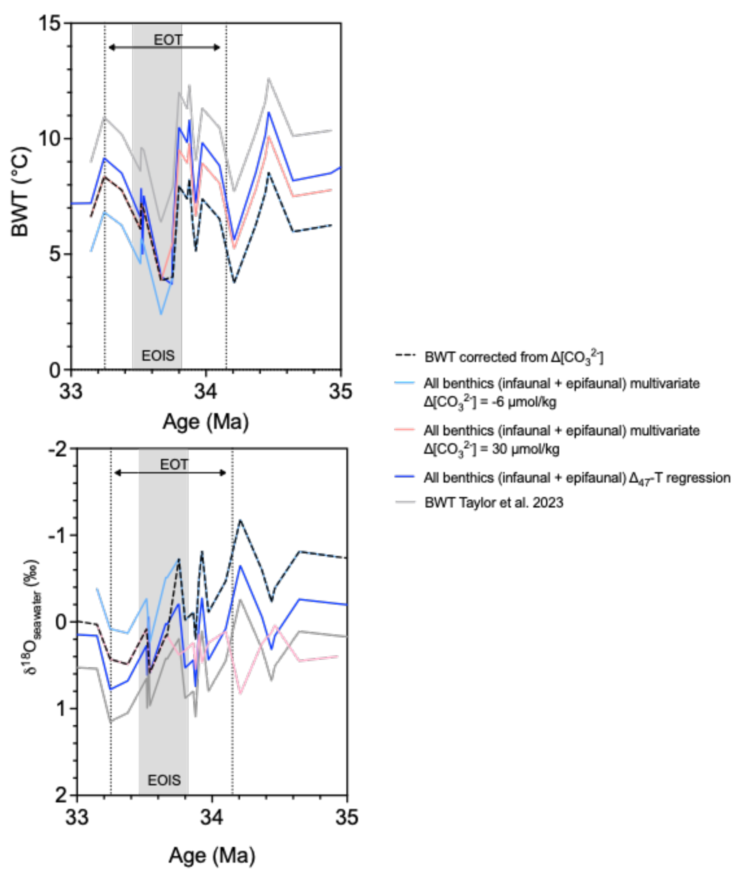

Compared to Taylor et al. (2023), the absolute temperatures are cooler, the amplitude of cooling associated with the EOIS is reduced, and changes in $\delta^{18}O_{sw}$ with the EOIS are positive and reasonable in magnitude (Supporting Information Table S10). At ~33.65 Ma, the coolest temperatures of the transition are reconstructed, with absolute bottom water temperatures estimated as 3.9 °C, instead of 6.5 °C. We estimate a cooling of 4.1 °C associated with the EOIS (Figure 9), rather than the 4.7 °C change reported by Taylor et al. (2023). These calculations use a pre- EOIS value of $\Delta[CO_3^{2-}]$ = -6 μmol/kg, and EOIS value of $\Delta[CO_3^{2-}]$ = 30 μmol/kg. The recalculated $\delta^{18}O_{sw}$ values (Figure 9, Supporting Information Table S10) support a positive excursion associated with the EOIS, as expected based on evidence for a major expansion of continental ice. The absolute values change from an average of -0.47 to 0.21 ‰ post-transition, with a change of 0.67 ‰, which is similar to the change in Taylor et al. (2023). The calculations do change the $\delta^{18}O_{sw}$ prior to the EOIS which is still closer to but still higher than anticipated based on theoretical calculations of and ice-free world (e.g., -0.9 to –1.2 ‰, Cramer et al., 2011), that could support the presence of some ice storage before this time.

3.5.3 Cooler Early Eocene Climatic Optimum temperatures from the new benthic Δ_{47}-temperature calibrations

Some of the warmest temperatures in the Cenozoic occurred during the Early Eocene Climatic Optimum (EECO; ~52 Ma), based on benthic foraminiferal $\delta^{18}O$ (Zachos et al. 2001). For the interval from 53 to 51 Ma, published (Meckler et al., 2022) Δ_{47}-temperatures for the Atlantic Ocean range from 10.4 to 20.6 °C and $\delta^{18}O_{sw}$ values range from –1.6 to 0.7 ‰, while average EECO temperatures estimated using benthic Δ_{47} are 16.2 °C and $\delta^{18}O_{sw}$ estimates average –0.3 ‰. These Δ_{47}-temperatures use the Meinicke et al. (2020) calibration and are 2-3 °C warmer than foraminiferal $\delta^{18}O$-based estimates, prompting studies to suggest there may be uncertainties in the calibration used, effects relating to carbonate chemistry, and/or warm saline deep water (Meckler et al., 2022; Daeron and Gray, 2023; Rohling et al., 2024).

Using the new benthic Δ_{47}-temperature regressions yields temperatures that are about ~1°C cooler, with temperatures ranging from 8.6 to 23.7 °C for the Early Eocene (Figure 10, Supporting Information Table S9). Average EECO temperatures of 14.6 °C and seawater $\delta^{18}O_{sw}$ values of -0.64 ‰ are estimated using the "all foraminifera" calibration, while values of 15.3 °C and -0.51 ‰ are reconstructed using the "all benthics (infaunal + epifaunal)" calibration, values of 16.1°C and -0.34 ‰ from the "epifaunal" calibration and 15.0 °C and -0.58 ‰ from the "infaunal" calibration (Figure 9, Supporting Information Table S9). With a pH correction for carbonate $\delta^{18}O$ as described in Meckler et al. (2022), the $\delta^{18}O_{sw}$ decreases further and is closer to expected ice-free predictions of the early Eocene of ~ 0.9 ‰ (Figure 10, Supporting Information Table S9) (Cramer et al., 2011). These new temperature estimates are slightly higher than Mg/Ca-derived bottom water temperatures at ODP Site 1263 in the Atlantic, where an average bottom water temperature of 14°C was reported (Lauretano et al., 2018) and are still warmer than $\delta^{18}O$-based temperatures (Meckler et al., 2022; Daeron and Gray, 2023; Rohling et al., 2024).

3.5.4 Cooler Paleocene temperatures from the new benthic Δ_{47}-temperature calibrations

Similar to the early Eocene, the Paleocene is characterized by warm global temperatures and ended with the first of a series of hyperthermals defining the transition into the Eocene, the Paleocene-Eocene Thermal Maximum (PETM) (Zachos et al. 2001). For the interval from 65 to 56 Ma, published (Meckler et al., 2022) Δ_{47}-temperatures for the Atlantic Ocean range from 10.9 to 19.9 °C and $\delta^{18}O_{sw}$ values range from -0.35 to 1.33 ‰, while average temperatures estimated using benthic Δ_{47} are 15.2 °C and $\delta^{18}O_{sw}$ estimates average 0.45 ‰. These Δ_{47}-temperatures use the Meinicke et al. (2020) planktic calibration and are also 2-3 °C warmer than foraminiferal $\delta^{18}O$-based estimates (Meckler et al., 2022; Daeron and Gray, 2023; Rohling et al., 2024).

Applying the new benthic Δ_{47}-temperature regressions to the published Δ_{47} data yields temperatures that are about ~1.5 °C cooler than what was originally reconstructed (Figure 10, Supporting Information Table S9). Average Paleocene temperatures of 13.6 °C and seawater $\delta^{18}O_{sw}$ values of 0.10 ‰ are estimated using the "all foraminifera" calibration, while values of 14.2 °C and 0.61 ‰ are reconstructed using the "all benthic-MB" calibration, values of 14.9 °C and 0.22 ‰ from the 'epifaunal" calibration and 13.9 °C and

0.37 ‰ from the "infaunal" calibration (Figure 10). With a pH correction for carbonate $\delta^{18}O$ as described in Meckler et al. (2022), the $\delta^{18}O_{sw}$ values decrease to be closer to ice-free predictions (Figure 11e, Supporting Information Table S9). These new estimates are similar to Mg/Ca-derived bottom water temperatures at during the Paleocene (e.g. Cramer et al., 2011) although still warmer than $\delta^{18}O$-based temperatures (Meckler et al., 2022; Daeron and Gray, 2023; Rohling et al., 2024).

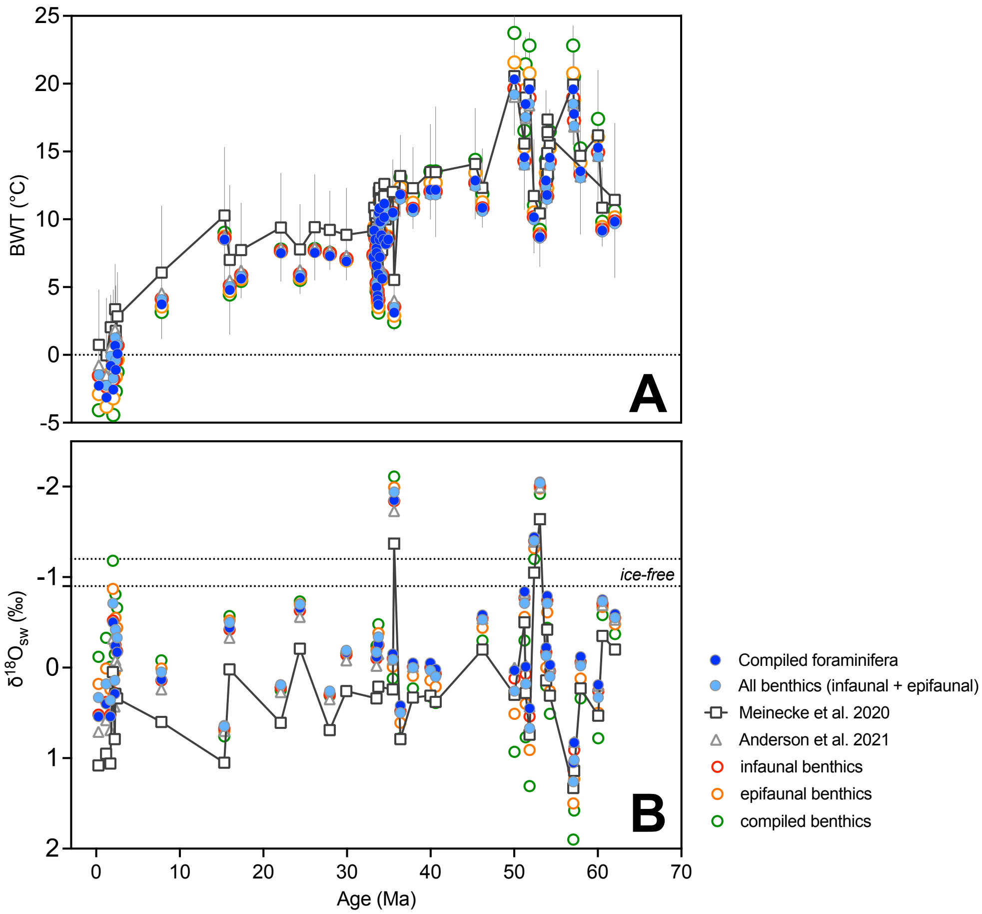

Figure 10: Comparison of recalculated bottom water temperatures and $\delta^{18}O_{sw}$ with clumped isotope data from Meckler et al. (2022). A) Bottom water temperature (BWT) reconstructions. B) $\delta^{18}O_{sw}$ reconstructions. Temperatures calculated with the new regressions from this study temp to decrease temperatures relative to the Meinicke et al. (2020) calibration. $\delta^{18}O_{sw}$ estimates also decrease with the new calibrations, however the decrease does not itself reconcile the deviation from ice-free predicted $\delta^{18}O_{sw}$ in the early Cenozoic.

3.5.5 Potential effects on Paleocene-Eocene Thermal Maximum (PETM) Δ_{47}-temperatures

Although there currently are no clumped isotope reconstructions published for the PETM, here, we conduct a preliminary assessment of the potential magnitude of effects on Δ_{47}-temperatures. We used $[CO_3^{2-}]$ from Zeebe and Zachos (2007) from nine sites, $[CO_3^{2-}]_{sat}$ based on site paleodepths, and the epifaunal benthics multivariable regression to explore the magnitude of potential temperature biases (Table 5). Temperature biases from site-specific $\Delta[CO_3^{2-}]$ values were calculated for three temperatures (15, 20, 35 °C), and are presented in Table 5. For example, the bias in temperature from $\Delta[CO_3^{2-}]$ ranging from -25 to -5 µmol/kg could lead to a PETM temperature overestimation by 3.2 to 4.3 °C, at a reconstructed temperature of 15°C (Table 5). Coupling Δ_{47} with site-specific estimates of $\Delta[CO_3^{2-}]$ would facilitate the most accurate determinations of temperature.

Figure 11: Comparison of recalculated bottom water temperatures and $\delta^{18}O_{sw}$ with clumped isotope data from Meckler et al. (2022). pCO2 estimates and TA estimates used to calculate $\Delta[CO_3^{2-}]$ B) $[CO_3^{2-}]$ values calculated as described in section 3.5.4a C) BWT reconstructions using the All benthic (infaunal + epifaunal) equations where non-corrected are the results of the Deming regression, and corrected are results from the multivariate regression. D) $\delta^{18}O_{sw}$ reconstructions with E) $\delta^{18}O_{sw}$ reconstructions with a pH correction in $\delta^{18}O_{carb}$ as described in Meckler et al. (2022).

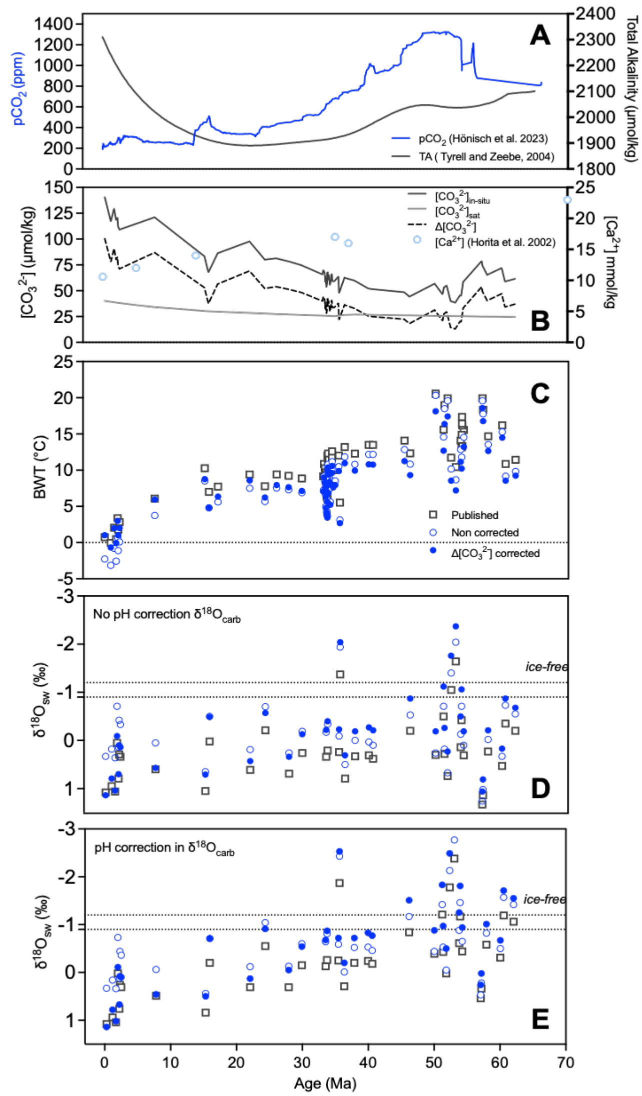

3.6 Key takeaways and recommendations for future studies

By roughly doubling the amount of foraminiferal calibration data through new analyses where we measured small samples using the latest analytical procedures and instrumentation, and utilizing the I-CDES reference frame, we are able to rigorously determine temperature calibrations for foraminiferal Δ_{47} with reduced uncertainties and also compare results to a large compilation of synthetic calcite Δ_{47} data over a similar temperature range. We observed no significant difference between the synthetic calcite regression and the composite foraminiferal calibration, consistent with prior findings.

We investigated non-thermal effects using multiple statistical methods and found evidence for weak dependencies on carbonate chemistry. R model selection analysis indicated the carbonate ion saturation of bottom waters has an impact on the Δ_{47} of planktic foraminifera which could result from dissolution. For benthic foraminiferal reconstructions, we found epifaunal and infaunal data have overlapping confidence bands. The benthic foraminiferal data analyzed here shows a correlation between Δ_{47} residuals and carbonate ion saturation within the overall dataset and in epifaunal benthic foraminifera.

Table 5: Estimates of potential PETM temperature biases on temperatures, assuming a carbonate ion effect on calcification as described by the multivariable regression for epifaunal benthics. $\Delta[CO_3^{2-}]$ for individual sites over the PETM estimated from Zeebe and Zachos (2007). The bias in temperature is based on, and is calculated using the difference in temperatures calculated using the $\Delta[CO_3^{2-}]$ = 50 µmol/kg (reference) and the calculated $\Delta[CO_3^{2-}]$ is specific to each site.

Sites	1266C	999	1001	690	1209B	1210B	1211C	1220B	1221C
$[CO_3^{2-}]$ (µmol/kg)	*37*	*<37*	*<37*	*48*	*52*	*54*	*58*	*49*	*50*
$[CO_3^{2-}]$sat (µmol/kg)	*62*	*55*	*57*	*57*	*59*	*62*	*63*	*63*	*67*
$\Delta[CO_3^{2-}]$ (µmol/kg)	*-25*	*-18*	*-20*	*-9*	*-7*	*-8*	*-5*	*-14*	*-17*
Possible biases:									
T = 15 (°C)	4.3	3.9	4.0	3.4	3.3	3.3	3.2	3.7	3.8
T = 20 (°C)	4.5	4.1	4.2	3.6	3.4	3.5	3.3	3.9	4.0
T = 35 (°C)	5.2	4.7	4.9	4.1	4.0	4.1	3.9	4.5	4.7

For planktic reconstructions, we recommend use of the composite foraminiferal calibration for temperature reconstructions due to the large sample size (n = 260) and the relevant temperature range for paleoceanographic reconstructions ($\Delta_{47} = 0.0374 \pm 0.0013\ 10^6/T^2 + 0.1744 \pm 0.0154$). We applied this calibration (and others) to core-top planktics in order to assess the ability of the thermometer to accurately constrain vertical hydrographic profiles for several regions, and this equation typically yields results that are the most accurate. Future studies should investigate any potential species-specific dissolution effects through analysis of transect data or dissolution experiments, and planktic reconstructions could explore the possible scope for dissolution impacts.

For benthic reconstructions, we recommend using the all foraminiferal calibration (no mixed benthics) ($\Delta_{47} = 0.0383 \pm 0.0013\ 10^6/T^2 + 0.1635 \pm 0.0154$) or the all benthics calibration (epifaunal and infaunal) ($\Delta_{47} = 0.0342 \pm 0.0034\ 10^6/T^2 + 0.2149 \pm 0.0431$), given the uncertainties associated with the mixed benthic samples. If $\Delta[CO_3^{2-}]$ can be constrained, through modeling and/or with proxy constraints from Li/Ca or B/Ca, the multivariate all benthics (epifaunal and infaunal) calibration can be used ($\Delta_{47} = 0.03865 \pm 0.00376\ 10^6/T^2 + 0.1518 \pm 0.0493 + 0.0001495 \pm 0.0000601$). We also suggest combining estimates of Δ_{47} -temperature derived using this approach with carbonate $\delta^{18}O$ estimates that factor in pH effects on carbonate $\delta^{18}O$, similar to the approach described in Meckler et al. (2022) to calculate seawater $\delta^{18}O$.

4 Conclusions

This study presents new clumped isotope data for foraminiferal core-tops made using recently established best practices with a meta-analysis of published data reported on the same reference frame. By performing a meta-analysis of planktic and benthic foraminiferal species, we determine possible factors that contribute to variance in Δ_{47}. The lab-specific data and meta-analysis do not show any species-specific offsets. Notably, non-thermal effects, including foraminiferal type and bottom water saturation, dataset and depth, and dataset and photosymbiont presence/absence, only explain ~13% of the variance. However, we show there is evidence for a weak carbonate ion effect on benthic foraminifera.

The regressions described in this study allow for benthic Δ_{47}-based temperature reconstructions to align more reasonably with published $\delta^{18}O$ estimates of bottom water temperatures and inferred climatologies throughout the Cenozoic. In particular, the application of a multivariate regression accounting for a weak carbonate ion effect in benthic foraminifera allows for a first-order investigation of how changes in $\Delta[CO_3^{2-}]$ affect Δ_{47}-based reconstructions for the Pleistocene, Eocene-Oligocene Transition, Early Eocene Climatic Optimum, and late Paleocene. We find that applying this calibration brings both temperature and calculated $\delta^{18}O_{sw}$ into better agreement with model-based deconvolution of benthic foraminiferal carbonate $\delta^{18}O$.

Based on our reconstructions we recommend the use of the composite foraminiferal calibration due to the sample size for planktonic foraminifera reconstructions ($\Delta_{47} = 0.0374 \pm 0.0013\ 10^6/T^2 + 0.1744 \pm 0.0154$), and the regression of the benthic foraminiferal calibration with mixed benthics removed for benthic reconstructions ($\Delta_{47} = 0.0342 \pm 0.0034\ 10^6/T^2 + 0.2149 \pm 0.0431$). For benthic foraminifera, when constraints on $\Delta[CO_3^{2-}]$ are available, we recommend the multivariate all benthic (infaunal + epifaunal) calibration for reconstructions ($\Delta_{47} = 0.03865 \pm 0.00376\ 10^6/T^2 + 0.1518 \pm 0.0493 + 0.0001495 \pm 0.0000601$).

Author contribution statement

A.T., H.T., and A.V. are joint first authors. Conceptualization: A.T., Data curation: A.T., H.T., A.A., C.R.P., H.C., Formal analysis: A.T., H.T., A.V., A.A., B.Z., C.T., C.B., D.B., D.S., F.C., H.C., I.M., J.C., M.G., M.K., R.F., R.E., R.C., Funding acquisition: A.T., R.E., R.C., Investigation, Methodology, and Visualization: A.T., H.T., A.V., C.T., C.B., H.C., I.M., M.G., R.F., R.E., R.C., Resources: A.T., D.S., F.C., J.L.S., M.K., R.E., R.C., T.M., Supervision: A.T., R.C., Validation: A.T., Writing – original draft: A.T., H.T., A.V., C.T., C.B., D.B., H.C., I.M., M.G., Writing – reviewing and editing: All co-authors.

Acknowledgments

We thank Eagle-Tripati lab members past and present for their work running standards, efforts in data entry and mass spectrometry, and contributions to discussions, Cynthia Ulloa, Lina Savage, Lorna Avila, and T.-Y. Chiang with sample preparation, and Ben Elliott for analytical support. This work was funded by Heising-Simons Foundation grant 2022-3314, DOE BES grant DE-FG02-83613ER16402, and NSF grants EAR-0949191, EAR-1352212, and RISE-228198 to Aradhna Tripati and RISE-2024426 to Robert Eagle. All UCLA and Fort Valley State University early career researchers were supported from fellowships granted by The Center for Diverse Leadership in Science supported by the Packard Foundation, Sloan Foundation, Silicon Valley Community Foundation, the Waverley Street Foundation, and NSF (RISE-228198). Hannah Tandy received support from a Schlanger IODP Fellowship, Alexandrea Arnold from a Cota-Robles Fellowship, Hannah Carroll from a NIH IRACDA Fellowship, and Robert Ulrich from an NSF GRFP.

Open Research

All data are in the Supporting Information associated with this paper. In addition, on publication, all data will be archived in Pangaea and EarthChem.

References

Agterhuis, T., Ziegler, M., de Winter, N. J., and Lourens, L. J. (2022). Warm deep-sea temperatures across Eocene Thermal Maximum 2 from clumped isotope thermometry. *Communications Earth and Environment*, *3*(1), 1–9. https://doi.org/10.1038/s43247-022-00350-8

Anand, P., Elderfield, H., and Conte, M. H. (2003). Calibration of Mg/Ca thermometry in planktic foraminifera from a sediment trap time series. *Paleoceanography*, *18*(2), 1050. https://doi.org/10.1029/2002PA000846

Anderson, N. T., Kelson, J. R., Kele, S., Daëron, M., Bonifacie, M., Horita, J., et al. (2021). A Unified Clumped Isotope Thermometer Calibration (0.5–1,100°C) Using Carbonate-Based Standardization. *Geophysical Research Letters*, *48*(7), e2020GL092069. https://doi.org/10.1029/2020GL092069

Bard, E. (2000). Hydrological Impact of Heinrich Events in the Subtropical Northeast Atlantic. *Science*, *289*, 1321–1324. https://doi.org/10.1126/science.289.5483.1321

Bard, E., Rostek, F., and Sonzogni, C. (1997). Interhemispheric synchrony of the last deglaciation inferred from alkenone palaeothermometry. *Nature*, *385*(6618), 707–710. https://doi.org/10.1038/385707a0

Barker, S., Greaves, M., and Elderfield, H. (2003). A study of cleaning procedures used for foraminiferal Mg/Ca paleothermometry. *Geochemistry, Geophysics, Geosystems*, *4*(9), 8407. https://doi.org/10.1029/2003GC000559

Barker, S., Cacho, I., Benway, H., and Tachikawa, K. (2005). Planktic foraminiferal Mg/Ca as a proxy for past oceanic temperatures: a methodological overview and data compilation for the Last Glacial Maximum. *Quaternary Science Reviews*, *24*(7), 821–834. https://doi.org/10.1016/j.quascirev.2004.07.016

Bartoń, K. (2022). MuMIn: Multi-model inference (2020). [R package version 1.5].

Bemis, B. E., Spero, H. J., Bijma, J., and Lea, D. W. (1998). Reevaluation of the oxygen isotopic composition of planktic foraminifera: Experimental results and revised paleotemperature equations. *Paleoceanography*, *13*(2), 150–160. https://doi.org/10.1029/98PA00070

Bernasconi, S. M., Müller, I. A., Bergmann, K. D., Breitenbach, S. F. M., Fernandez, A., Hodell, D. A., et al. (2018). Reducing Uncertainties in Carbonate Clumped Isotope Analysis Through Consistent Carbonate-Based Standardization. *Geochemistry, Geophysics, Geosystems*, *19*(9), 2895–2914. https://doi.org/10.1029/2017GC007385

Bernasconi, S. M., Daëron, M., Bergmann, K. D., Bonifacie, M., Meckler, A. N., Affek, H. P., et al. (2021). InterCarb: A Community Effort to Improve Interlaboratory Standardization of the Carbonate Clumped Isotope Thermometer Using Carbonate Standards. *Geochemistry, Geophysics, Geosystems*, *22*(5), e2020GC009588. https://doi.org/10.1029/2020GC009588

Bian, N., and Martin, P. A. (2010). Investigating the fidelity of Mg/Ca and other elemental data from reductively cleaned planktic foraminifera. *Paleoceanography*, *25*(2). https://doi.org/10.1029/2009PA001796

Breitenbach, S. F. M., Mleneck-Vautravers, M. J., Grauel, A.-L., Lo, L., Bernasconi, S. M., Müller, I. A., et al. (2018). Coupled Mg/Ca and clumped isotope analyses of foraminifera provide consistent water temperatures. *Geochimica et Cosmochimica Acta*, *236*, 283–296. https://doi.org/10.1016/j.gca.2018.03.010

Came, R. E., Oppo, D. W., and McManus, J. F. (2007). Amplitude and timing of temperature and salinity variability in the subpolar North Atlantic over the past 10 k.y. *Geology*, *35*(4), 315–318. https://doi.org/10.1130/G23455A.1

Conte, M. H., Weber, J. C., King, L. L., and Wakeham, S. G. (2001). The alkenone temperature signal in western North Atlantic surface waters. *Geochimica et Cosmochimica Acta*, *65*(23), 4275–4287. https://doi.org/10.1016/S0016-7037(01)00718-9

Conte, M. H., Sicre, M.-A., Rühlemann, C., Weber, J. C., Schulte, S., Schulz-Bull, D., and Blanz, T. (2006). Global temperature calibration of the alkenone unsaturation index (UK′37) in surface waters and comparison with surface sediments. *Geochemistry, Geophysics, Geosystems*, *7*(2), Q02005. https://doi.org/10.1029/2005GC001054

Coxall, H. K., Wilson, P. A., Pälike, H., Lear, C. H., and Backman, J. (2005). Rapid stepwise onset of Antarctic glaciation and deeper calcite compensation in the Pacific Ocean. *Nature*, *433*(7021), 53–57. https://doi.org/10.1038/nature03135

Cramer, B. S., Miller, K. G., Barrett, P. J., and Wright, J. D. (2011). Late Cretaceous–Neogene trends in deep ocean temperature and continental ice volume: Reconciling records of benthic foraminiferal geochemistry (δ^{18}O and Mg/Ca) with sea level history. *Journal of Geophysical Research: Oceans*, *116*(C12). https://doi.org/10.1029/2011JC007255

Daëron, M., and Gray, W. R. (2023). Revisiting Oxygen-18 and Clumped Isotopes in Planktic and Benthic Foraminifera. *Paleoceanography and Paleoclimatology*, *38*(10), e2023PA004660. https://doi.org/10.1029/2023PA004660

Daëron, M., Blamart, D., Peral, M., and Affek, H. P. (2016). Absolute isotopic abundance ratios and the accuracy of Δ47 measurements. *Chemical Geology*, *442*, 83–96. https://doi.org/10.1016/j.chemgeo.2016.08.014

Darling, K. F., Wade, C. M., Siccha, M., Trommer, G., Schulz, H., Abdolalipour, S., and Kurasawa, A. (2017). Genetic diversity and ecology of the planktic foraminifers *Globigerina bulloides*, *Turborotalita quinqueloba* and *Neogloboquadrina pachyderma* off the Oman margin during the late SW Monsoon. *Marine Micropaleontology*, *137*, 64–77. https://doi.org/10.1016/j.marmicro.2017.10.006

Dawber, C. F., and Tripati, A. (2012). Relationships between bottom water carbonate saturation and element/Ca ratios in coretop samples of the benthic foraminifera *Oridorsalis umbonatus*. *Biogeosciences*, *9*(8), 3029–3045. https://doi.org/10.5194/bg-9-3029-2012

Defliese, W. F., and Lohmann, K. C. (2015). Non-linear mixing effects on mass-47 CO_2 clumped isotope thermometry: Patterns and implications. *Rapid Communications in Mass Spectrometry*, *29*(9), 901–909. https://doi.org/10.1002/rcm.7175

Defliese, W. F., and Tripati, A. (2020). Analytical effects on clumped isotope thermometry: Comparison of a common sample set analyzed using multiple instruments, types of standards, and standardization windows. *Rapid Communications in Mass Spectrometry*, *34*(8), e8666. https://doi.org/10.1002/rcm.8666

Dennis, K. J., Affek, H. P., Passey, B. H., Schrag, D. P., and Eiler, J. M. (2011). Defining an absolute reference frame for 'clumped' isotope studies of CO_2. *Geochimica et Cosmochimica Acta*, *75*(22), 7117–7131. https://doi.org/10.1016/j.gca.2011.09.025

Dickson, A. G., Sabine, C. L., Christian, J. R., Bargeron, C. P., and North Pacific Marine Science Organization (Eds.). (2007). Guide to best practices for ocean CO_2 measurements. Sidney, BC: North Pacific Marine Science Organization.

Elderfield, H., and Ganssen, G. (2000). Past temperature and δ18O of surface ocean waters inferred from foraminiferal Mg/Ca ratios. *Nature*, *405*(6785), 442–445. https://doi.org/10.1038/35013033

Elderfield, H., Yu, J., Anand, P., Kiefer, T., and Nyland, B. (2006). Calibrations for benthic foraminiferal Mg/Ca paleothermometry and the carbonate ion hypothesis. *Earth and Planetary Science Letters*, *250*(3), 633–649. https://doi.org/10.1016/j.epsl.2006.07.041

Evans, D., Sagoo, N., Renema, W., Cotton, L. J., Müller, W., Todd, J. A., et al. (2018). Eocene greenhouse climate revealed by coupled clumped isotope-Mg/Ca thermometry. *Proceedings of the National Academy of Sciences*, *115*(6), 1174–1179. https://doi.org/10.1073/pnas.1714744115

Ferguson, J. E., Henderson, G. M., Kucera, M., and Rickaby, R. E. M. (2008). Systematic change of foraminiferal Mg/Ca ratios across a strong salinity gradient. *Earth and Planetary Science Letters*, *265*(1), 153–166. https://doi.org/10.1016/j.epsl.2007.10.011

Fox, J., and Weisberg, S. (2019). Using car functions in other functions. [CRAN R].

de Garidel-Thoron, T., Rosenthal, Y., Bassinot, F., and Beaufort, L. (2005). Stable sea surface temperatures in the western Pacific warm pool over the past 1.75 million years. *Nature*, *433*(7023), 294–298. https://doi.org/10.1038/nature03189

Ghosh, P., Adkins, J., Affek, H., Balta, B., Guo, W., Schauble, E. A., et al. (2006). ^{13}C–^{18}O bonds in carbonate minerals: A new kind of paleothermometer. *Geochimica et Cosmochimica Acta*, *70*(6), 1439–1456. https://doi.org/10.1016/j.gca.2005.11.014

de Goeyse, S., Webb, A. E., Reichart, G.-J., and de Nooijer, L. J. (2021). Carbonic anhydrase is involved in calcification by the benthic foraminifer *Amphistegina lessonii*. *Biogeosciences*, *18*(2), 393–401. https://doi.org/10.5194/bg-18-393-2021

Grauel, A.-L., Schmid, T. W., Hu, B., Bergami, C., Capotondi, L., Zhou, L., and Bernasconi, S. M. (2013). Calibration and application of the 'clumped isotope' thermometer to foraminifera for high-resolution climate reconstructions. *Geochimica et Cosmochimica Acta*, *108*, 125–140. https://doi.org/10.1016/j.gca.2012.12.049

Gray, W. R., and Evans, D. (2019). Nonthermal Influences on Mg/Ca in Planktic Foraminifera: A Review of Culture Studies and Application to the Last Glacial Maximum. *Paleoceanography and Paleoclimatology*, *34*(3), 306–315. https://doi.org/10.1029/2018PA003517

Greaves, M., Caillon, N., Rebaubier, H., Bartoli, G., Bohaty, S., Cacho, I., et al. (2008). Interlaboratory comparison study of calibration standards for foraminiferal Mg/Ca thermometry. *Geochemistry, Geophysics, Geosystems*, *9*(8), Q08010. https://doi.org/10.1029/2008GC001974

Guo, W. (2020). Kinetic clumped isotope fractionation in the DIC-H_2O-CO_2 system: Patterns, controls, and implications. *Geochimica et Cosmochimica Acta*, *268*, 230–257. https://doi.org/10.1016/j.gca.2019.07.055

Haynes, L. L., Hönisch, B., Holland, K., Eggins, S., Rosenthal, Y. (2023). Calibrating non-thermal effects on planktic foraminiferal Mg/Ca for application across the Cenozoic. Paleoceanography and Paleoclimatology, 38, e2023PA004613.

Hill, P. S., Tripati, A. K., and Schauble, E. A. (2014). Theoretical constraints on the effects of pH, salinity, and temperature on clumped isotope signatures of dissolved inorganic carbon species and precipitating carbonate minerals. *Geochimica et Cosmochimica Acta*, *125*, 610–652. https://doi.org/10.1016/j.gca.2013.06.018

Hönisch, B., Allen, K. A., Lea, D. W., Spero, H. J., Eggins, S. M., Arbuszewski, J., et al. (2013). The influence of salinity on Mg/Ca in planktic foraminifers – Evidence from cultures, core-top sediments and complementary $\delta^{18}O$. *Geochimica et Cosmochimica Acta*, *121*, 196–213. https://doi.org/10.1016/j.gca.2013.07.028

Hoogakker, B. A. A., Klinkhammer, G. P., Elderfield, H., Rohling, E. J., and Hayward, C. (2009). Mg/Ca paleothermometry in high salinity environments. *Earth and Planetary Science Letters*, *284*(3), 583–589. https://doi.org/10.1016/j.epsl.2009.05.027

Ishimura, T., Tsunogai, U., Hasegawa, S., Nakagawa, F., Oi, T., Kitazato, H., et al. (2012). Variation in stable carbon and oxygen isotopes of individual benthic foraminifera: tracers for quantifying the magnitude of isotopic disequilibrium. *Biogeosciences*, *9*(11), 4353–4367. https://doi.org/10.5194/bg-9-4353-2012

Jautzy, J. J., Savard, M. M., Dhillon, R. S., Bernasconi, S. M., and Smirnoff, A. (2020). Clumped isotope temperature calibration for calcite: Bridging theory and experimentation. *Geochemical Perspectives Letters*, *14*, 36–41. https://doi.org/10.7185/geochemlet.2021

Jentzen, A., Nürnberg, D., Hathorne, E. C., and Schönfeld, J. (2018). Mg/Ca and $\delta^{18}O$ in living planktic foraminifers from the Caribbean, Gulf of Mexico and Florida Straits. Biogeosciences, 15(23), 7077-7095.

John, C. M., and Bowen, D. (2016). Community software for challenging isotope analysis: First applications of 'Easotope' to clumped isotopes. *Rapid Communications in Mass Spectrometry*, *30*(21), 2285–2300. https://doi.org/10.1002/rcm.7720

Kelson, J. R., Huntington, K. W., Schauer, A. J., Saenger, C., and Lechler, A. R. (2017). Toward a universal carbonate clumped isotope calibration: Diverse synthesis and preparatory methods suggest a single temperature relationship. *Geochimica et Cosmochimica Acta*, *197*, 104–131. https://doi.org/10.1016/j.gca.2016.10.010

Kim, J.-H., Schouten, S., Hopmans, E. C., Donner, B., and Sinninghe Damsté, J. S. (2008). Global sediment core-top calibration of the TEX_{86} paleothermometer in the ocean. *Geochimica et Cosmochimica Acta*, *72*(4), 1154–1173. https://doi.org/10.1016/j.gca.2007.12.010

Kim, S.-T., and O'Neil, J. R. (1997). Equilibrium and nonequilibrium oxygen isotope effects in synthetic carbonates. *Geochimica et Cosmochimica Acta*, *61*(16), 3461–3475. https://doi.org/10.1016/S0016-7037(97)00169-5

Kluge, T., John, C. M., Jourdan, A.-L., Davis, S., and Crawshaw, J. (2015). Laboratory calibration of the calcium carbonate clumped isotope thermometer in the 25–250 °C temperature range. *Geochimica et Cosmochimica Acta*, *157*, 213–227. https://doi.org/10.1016/j.gca.2015.02.028

Koutavas, A. (2002). El Nino-Like Pattern in Ice Age Tropical Pacific Sea Surface Temperature. *Science*, *297*(5579), 226–230. https://doi.org/10.1126/science.1072376

Lea, D. W., Mashiotta, T. A., and Spero, H. J. (1999). Controls on magnesium and strontium uptake in planktic foraminifera determined by live culturing. *Geochimica et Cosmochimica Acta*, *63*(16), 2369–2379. https://doi.org/10.1016/S0016-7037(99)00197-0

Lea, D. W., Martin, P. A., Pak, D. K., and Spero, H. J. (2002). Reconstructing a 350ky history of sea level using planktic Mg/Ca and oxygen isotope records from a Cocos Ridge core. *Quaternary Science Reviews*, *21*(1), 283–293. https://doi.org/10.1016/S0277-3791(01)00081-6

Lear, C. H., and Rosenthal, Y. (2006). Benthic foraminiferal Li/Ca: Insights into Cenozoic seawater carbonate saturation state. *Geology*, *34*(11), 985–988. https://doi.org/10.1130/G22792A.1

Lear, C. H., Mawbey, E. M., and Rosenthal, Y. (2010). Cenozoic benthic foraminiferal Mg/Ca and Li/Ca records: toward unlocking temperatures and saturation states. *Paleoceanography*, *25*(4). https://doi.org/10.1029/2009PA001880

LeGrande, A. N., and Schmidt, G. A. (2006). Global gridded data set of the oxygen isotopic composition in seawater. *Geophysical Research Letters*, *33*(12). https://doi.org/10.1029/2006GL026011

Leider, A., Hinrichs, K.-U., Mollenhauer, G., and Versteegh, G. J. M. (2010). Core-top calibration of the lipid-based $U_{37}^{K'}$ and TEX_{86} temperature proxies on the southern Italian shelf (SW Adriatic Sea, Gulf of Taranto). *Earth and Planetary Science Letters*, *300*(1), 112–124. https://doi.org/10.1016/j.epsl.2010.09.042

Leutert, T. J., Sexton, P. F., Tripati, A., Piasecki, A., Ho, S. L., and Meckler, A. N. (2019). Sensitivity of clumped isotope temperatures in fossil benthic and planktic foraminifera to diagenetic alteration. *Geochimica et Cosmochimica Acta*, *257*, 354–372. https://doi.org/10.1016/j.gca.2019.05.005

Leutert, T. J., Auderset, A., Martínez-García, A., Modestou, S., and Meckler, A. N. (2020). Coupled Southern Ocean cooling and Antarctic ice sheet expansion during the middle Miocene. *Nature Geoscience*, *13*(9), 634–639. https://doi.org/10.1038/s41561-020-0623-0

Levitus, S., Locarnini, R. A., Boyer, T. P., Mishonov, A. V., Antonov, J. I., Garcia, H. E., et al. (2010). World ocean atlas 2009. Retrieved from https://repository.library.noaa.gov/view/noaa/1259

Lucarelli, J. K., Carroll, H. M., Ulrich, R. N., Elliott, B. M., Coplen, T. B., Eagle, R. A., and Tripati, A. (2023). Equilibrated Gas and Carbonate Standard-Derived Dual (Δ_{47} and Δ_{48}) Clumped Isotope Values. *Geochemistry, Geophysics, Geosystems*, *24*(2), e2022GC010458. https://doi.org/10.1029/2022GC010458

Lucarelli, J. K., Purgstaller, B., Parven, Z., Watkins, J. M., Eagle, R., Dietzel, M., and Tripati, A. (2022). Paired Δ_{47} and Δ_{48} analyses and model calculations constrain equilibrium, experimentally-manipulated kinetic isotope effects, and mixing effects in calcite. Retrieved from https://eartharxiv.org/repository/view/3039/

Malevich, S. B., Vetter, L., and Tierney, J. E. (2019). Global Core Top Calibration of δ^{18}O in Planktic Foraminifera to Sea Surface Temperature. *Paleoceanography and Paleoclimatology*, *34*(8), 1292–1315. https://doi.org/10.1029/2019PA003576

Marchitto, T. M., Curry, W. B., Lynch-Stieglitz, J., Bryan, S. P., Cobb, K. M., and Lund, D. C. (2014). Improved oxygen isotope temperature calibrations for cosmopolitan benthic foraminifera. *Geochimica et Cosmochimica Acta*, *130*, 1–11. https://doi.org/10.1016/j.gca.2013.12.034

Martin, P. A., and Lea, D. W. (2002). A simple evaluation of cleaning procedures on fossil benthic foraminiferal Mg/Ca. *Geochemistry, Geophysics, Geosystems*, *3*(10), 1–8. https://doi.org/10.1029/2001GC000280

Mashiotta, T. A., Lea, D. W., and Spero, H. J. (1999). Glacial–interglacial changes in Subantarctic sea surface temperature and δ18O-water using foraminiferal Mg. *Earth and Planetary Science Letters*, *170*(4), 417–432. https://doi.org/10.1016/S0012-821X(99)00116-8

Meckler, A. N., Sexton, P. F., Piasecki, A. M., Leutert, T. J., Marquardt, J., Ziegler, M., et al. (2022). Cenozoic evolution of deep ocean temperature from clumped isotope thermometry. *Science*, *377*(6601), 86–90. https://doi.org/10.1126/science.abk0604

Meinicke, N., Ho, S. L., Hannisdal, B., Nürnberg, D., Tripati, A., Schiebel, R., and Meckler, A. N. (2020). A robust calibration of the clumped isotopes to temperature relationship for foraminifers. *Geochimica et Cosmochimica Acta*, *270*, 160–183. https://doi.org/10.1016/j.gca.2019.11.022

Müller, P. J., Kirst, G., Ruhland, G., von Storch, I., and Rosell-Melé, A. (1998). Calibration of the alkenone paleotemperature index U37K′ based on core-tops from the eastern South Atlantic and the global ocean (60°N-60°S). *Geochimica et Cosmochimica Acta*, *62*(10), 1757–1772. https://doi.org/10.1016/S0016-7037(98)00097-0

de Nooijer, L. J., Spero, H. J., Erez, J., Bijma, J., and Reichart, G. J. (2014). Biomineralization in perforate foraminifera. *Earth-Science Reviews*, *135*, 48–58. https://doi.org/10.1016/j.earscirev.2014.03.013

Nürnberg, D., Buma, J., and Hemleben, C. (1996). Assessing the reliability of magnesium in foraminiferal calcite as a proxy for water mass temperatures. *Geochimica et Cosmochimica Acta*, *60*(5), 803–814.

Olsen, A., Lange, N., Key, R. M., Tanhua, T., Álvarez, M., Becker, S., et al. (2019). GLODAPv2.2019 – an update of GLODAPv2. *Earth System Science Data*, *11*(3), 1437–1461. https://doi.org/10.5194/essd-11-1437-2019

Pak, D. K., Lea, D. W., and Kennett, J. P. (2004). Seasonal and interannual variation in Santa Barbara Basin water temperatures observed in sediment trap foraminiferal Mg/Ca. *Geochemistry, Geophysics, Geosystems*, *5*(12), Q12008. https://doi.org/10.1029/2004GC000760

Parvez, Z., Lucarelli, J., Matamoros, I. W., Rubi, J., Miguel, K., Elliott, B., et al. (2023). Dual carbonate clumped isotopes (Δ_{47}-Δ_{48}) constrains kinetic effects and timescales in peridotite-associated springs at the Cedars, Northern California. *Geochimica et Cosmochimica Acta*, *358*, 77–92.

Peck, V. L., Yu, J., Kender, S., and Riesselman, C. R. (2010). Shifting ocean carbonate chemistry during the Eocene-Oligocene climate transition: Implications for deep-ocean Mg/Ca paleothermometry. *Paleoceanography*, *25*(4), PA4219. https://doi.org/10.1029/2009PA001906

Peral, M., Daëron, M., Blamart, D., Bassinot, F., Dewilde, F., Smialkowski, N., et al. (2018). Updated calibration of the clumped isotope thermometer in planktic and benthic foraminifera. *Geochimica et Cosmochimica Acta*, *239*, 1–16. https://doi.org/10.1016/j.gca.2018.07.016

Petersen, S. V., Defliese, W. F., Saenger, C., Daëron, M., Huntington, K. W., John, C. M., et al. (2019). Effects of Improved ^{17}O Correction on Interlaboratory Agreement in Clumped Isotope Calibrations, Estimates of Mineral-Specific Offsets, and Temperature Dependence of Acid Digestion Fractionation. *Geochemistry, Geophysics, Geosystems*, *20*(7), 3495–3519. https://doi.org/10.1029/2018GC008127

Piasecki, A., Bernasconi, S. M., Grauel, A.-L., Hannisdal, B., Ho, S. L., Leutert, T. J., et al. (2019). Application of Clumped Isotope Thermometry to Benthic Foraminifera. *Geochemistry, Geophysics, Geosystems*, *20*(4), 2082–2090. https://doi.org/10.1029/2018GC007961

Powers, L., Werne, J. P., Vanderwoude, A. J., Sinninghe Damsté, J. S., Hopmans, E. C., and Schouten, S. (2010). Applicability and calibration of the TEX_{86} paleothermometer in lakes. *Organic Geochemistry*, *41*(4), 404–413. https://doi.org/10.1016/j.orggeochem.2009.11.009

Pusz, A. E., Thunell, R. C., and Miller, K. G. (2011). Deep water temperature, carbonate ion, and ice volume changes across the Eocene-Oligocene climate transition. *Paleoceanography*, *26*(2). https://doi.org/10.1029/2010PA001950

R Core Team. (2022). R: A language and environment for statistical computing. (Version 4.2.1). Vienna, Austria: R Foundation for Statistical Computing. Retrieved from https://www.R-project.org/

Rathman, S., and Kuhnert, H. (2008). Carbonate ion effect on Mg/Ca, Sr/Ca and stable isotopes on the benthic foraminifera *Oridorsalis umbonatus* off Namibia. *Marine Micropaleontology*, *66*(2), 120–133.

Regenberg, M., Steph, S., Nürnberg, D., Tiedemann, R., and Garbe-Schönberg, D. (2009). Calibrating Mg/Ca ratios of multiple planktic foraminiferal species with $\delta^{18}O$-calcification temperatures: Paleothermometry for the upper water column. *Earth and Planetary Science Letters*, *278*(3), 324–336. https://doi.org/10.1016/j.epsl.2008.12.019

Rippert, N., Nürnberg, D., Raddatz, J., Maier, E., Hathorne, E., Bijma, J., and Tiedemann, R. (2016). Constraining foraminiferal calcification depths in the western Pacific warm pool. *Marine Micropaleontology*, *128*, 14–27. https://doi.org/10.1016/j.marmicro.2016.08.004

Rohling, E.J., Gernon, T.M., Heslop, D., Reichart, G.J., Roberts, A.P. and Yu, J. (2024). Reconciling the apparent discrepancy between Cenozoic deep-sea temperatures from proxies and from benthic oxygen isotope deconvolution. *Paleoceanography and Paleoclimatology, 39*(11), p.e2024PA004872.

Román-Palacios, C., Carroll, H., Arnold, A., Flores, R., Petersen, S., McKinnon, K., and Tripati, A. (2021). BayClump: Bayesian Calibration and Temperature Reconstructions for Clumped Isotope Thermometry. *Earth and Space Science Open Archive*. https://doi.org/10.1002/essoar.10507995.1

Rosenthal, Y., Perron-Cashman, S., Lear, C. H., Bard, E., Barker, S., Billups, K., et al. (2004). Interlaboratory comparison study of Mg/Ca and Sr/Ca measurements in planktic foraminifera for paleoceanographic research. *Geochemistry, Geophysics, Geosystems*, *5*(4). https://doi.org/10.1029/2003GC000650

Russell, A. D., Hönisch, B., Spero, H. J., and Lea, D. W. (2004). Effects of seawater carbonate ion concentration and temperature on shell U, Mg, and Sr in cultured planktic foraminifera. *Geochimica et Cosmochimica Acta*, *68*(21), 4347–4361. https://doi.org/10.1016/j.gca.2004.03.013

Sachs, J. P., Schneider, R. R., Eglinton, T. I., Freeman, K. H., Ganssen, G., McManus, J. F., and Oppo, D. W. (2000). Alkenones as paleoceanographic proxies. *Geochemistry, Geophysics, Geosystems*, *1*(11). https://doi.org/10.1029/2000GC000059

Sadekov, A. Yu., Darling, K. F., Ishimura, T., Wade, C. M., Kimoto, K., Singh, A. D., et al. (2016). Geochemical imprints of genotypic variants of *Globigerina bulloides* in the Arabian Sea. *Paleoceanography*, *31*(10), 1440–1452. https://doi.org/10.1002/2016PA002947

Saenger, C. P., and Evans, M. N. (2019). Calibration and validation of environmental controls on planktic foraminifera Mg/Ca using global core-top data. Paleoceanography and Paleoclimatology, 34, 1249-1270.

Schauble, E. A., Ghosh, P., and Eiler, J. M. (2006). Preferential formation of ^{13}C–^{18}O bonds in carbonate minerals, estimated using first-principles lattice dynamics. *Geochimica et Cosmochimica Acta*, *70*(10), 2510–2529. https://doi.org/10.1016/j.gca.2006.02.011

Schiebel, R., and Hemleben, C. (2017). Planktic Foraminifers in the Modern Ocean. Berlin, Heidelberg: Springer Berlin Heidelberg. https://doi.org/10.1007/978-3-662-50297-6

Schouten, S., Huguet, C., Hopmans, E. C., Kienhuis, M. V. M., and Sinninghe Damsté, J. S. (2007). Analytical Methodology for TEX$_{86}$ Paleothermometry by High-Performance Liquid Chromatography/Atmospheric Pressure Chemical Ionization-Mass Spectrometry. *Analytical Chemistry*, *79*(7), 2940–2944. https://doi.org/10.1021/ac062339v

Shackleton, N. J. (1974). Attainment of isotopic equilibrium between ocean water and the benthonic foraminifera genus *Uvigerina*: isotopic changes in the ocean during the last glacial. *Cent. Nat. Rech. Schi. Colloq. Int.*, *219*, 203–209.

Shackleton, N. J., and Opdyke, N. D. (1973). Oxygen Isotope and Palaeomagnetic Stratigraphy of Equatorial Pacific Core V28-238: Oxygen Isotope Temperatures and Ice Volumes on a 10^5 Year and 10^6 Year Scale. *Quaternary Research*, *3*(1), 39–55. https://doi.org/10.1016/0033-5894(73)90052-5

Skinner, L. C., and Elderfield, H. (2005). Constraining ecological and biological bias in planktic foraminiferal Mg/Ca and $\delta^{18}O_{cc}$: A multispecies approach to proxy calibration testing. *Paleoceanography*, *20*(1). https://doi.org/10.1029/2004PA001058

Skinner, L. C., Elderfield, H., and Hall, M. (2007). Phasing of millennial climate events and Northeast Atlantic deep-water temperature change since 50 ka BP. *Ocean Circulation: Mechanisms and Impacts—Past and Future Changes of Meridional Overturning*, *173*, 197–208.

Spero, H. J., Bijma, J., Lea, D. W., and Bemis, B. E. (1997). Effect of seawater carbonate concentration on foraminiferal carbon and oxygen isotopes. *Nature*, *390*(6659), 497–500. https://doi.org/10.1038/37333

Stirpe, C. R., Allen, K. A., Sikes, E. L., Zhou, X., Rosenthal, Y., Cruz-Uribe, A. M., and Brooks, H. L. (2021). The Mg/Ca proxy for temperature: A Uvigerina core-top study in the Southwest Pacific. *Geochimica et Cosmochimica Acta*, *309*, 299–312. https://doi.org/10.1016/j.gca.2021.06.015

Swart, P. K., Lu, C., Moore, E. W., Smith, M. E., Murray, S. T., and Staudigel, P. T. (2021). A calibration equation between Δ_{48} values of carbonate and temperature. *Rapid Communications in Mass Spectrometry*, *35*(17), e9147. https://doi.org/10.1002/rcm.9147

Tang, J., Dietzel, M., Fernandez, A., Tripati, A. K., and Rosenheim, B. E. (2014). Evaluation of kinetic effects on clumped isotope fractionation (Δ_{47}) during inorganic calcite precipitation. *Geochimica et Cosmochimica Acta*, *134*, 120–136. https://doi.org/10.1016/j.gca.2014.03.005

Taylor, V. E., Wilson, P. A., Bohaty, S. M., and Meckler, A. N. (2023). Transient Deep Ocean Cooling in the Eastern Equatorial Pacific Ocean at the Eocene-Oligocene Transition. *Paleoceanography and Paleoclimatology*, *38*(8), e2023PA004650. https://doi.org/10.1029/2023PA004650

Thiagarajan, N., Adkins, J., and Eiler, J. (2011). Carbonate clumped isotope thermometry of deep-sea corals and implications for vital effects. *Geochimica et Cosmochimica Acta*, *75*(16), 4416–4425. https://doi.org/10.1016/j.gca.2011.05.004

Tierney, J. E., and Tingley, M. P. (2014). A Bayesian, spatially-varying calibration model for the TEX_{86} proxy. *Geochimica et Cosmochimica Acta*, *127*, 83–106. https://doi.org/10.1016/j.gca.2013.11.026

Tripati, A. K., Backman, J., Elderfield, H., and Ferretti, P. (2005). Eocene bipolar glaciation associated with global carbon cycle changes. *Nature*, *436*(7049), 341–346. https://doi.org/10.1038/nature03874

Tripati, A. K., Eagle, R. A., Thiagarajan, N., Gagnon, A. C., Bauch, H., Halloran, P. R., and Eiler, J. M. (2010). ^{13}C–^{18}O isotope signatures and 'clumped isotope' thermometry in foraminifera and coccoliths. *Geochimica et Cosmochimica Acta*, *74*(20), 5697–5717. https://doi.org/10.1016/j.gca.2010.07.006

Tripati, A. K., Sahany, S., Pittman, D., Eagle, R. A., Neelin, J. D., Mitchell, J. L., and Beaufort, L. (2014). Modern and glacial tropical snowlines controlled by sea surface temperature and atmospheric mixing. *Nature Geoscience*, *7*(3), 205–209. https://doi.org/10.1038/ngeo2082

Tripati, A. K., Hill, P. S., Eagle, R. A., Mosenfelder, J. L., Tang, J., Schauble, E. A., et al. (2015). Beyond temperature: Clumped isotope signatures in dissolved inorganic carbon species and the influence of solution chemistry on carbonate mineral composition. *Geochimica et Cosmochimica Acta*, *166*, 344–371. https://doi.org/10.1016/j.gca.2015.06.021

Upadhyay, D., Lucarelli, J., Arnold, A., Flores, R., Bricker, H., Ulrich, R. N., et al. (2021). Carbonate clumped isotope analysis (Δ_{47}) of 21 carbonate standards determined via gas-source isotope-ratio mass spectrometry on four instrumental configurations using carbonate-based standardization and multiyear data sets. *Rapid Communications in Mass Spectrometry*, *35*(17), e9143. https://doi.org/10.1002/rcm.9143

Yu, J., and Elderfield, H. (2008). Mg/Ca in the benthic foraminifera *Cibicidoides wuellerstorfi* and *Cibicidoides mundulus*: Temperature versus carbonate ion saturation. *Earth and Planetary Science Letters*, *276*(1), 129–139. https://doi.org/10.1016/j.epsl.2008.09.015

Zachos, J., Stott, L. D., and Lohmann, K. C. (1994). Evolution of Early Cenozoic marine temperatures. *Paleoceanography*, *9*(2), 353–387. https://doi.org/10.1029/93PA03266

Zachos, J., Pagani, M., Sloan, L., Thomas, E., and Billups, K. (2001). Trends, Rhythms, and Aberrations in Global Climate 65 Ma to Present. *Science*, *292*(5517), 686–693. https://doi.org/10.1126/science.1059412

Zachos, J., Dickens, G. R., and Zeebe, R. E. (2008). An early Cenozoic perspective on greenhouse warming and carbon-cycle dynamics. *Nature*, *451*(7176), 279–283. https://doi.org/10.1038/nature06588

Zeebe, R. E. (1999). An explanation of the effect of seawater carbonate concentration on foraminiferal oxygen isotopes. *Geochimica et Cosmochimica Acta*, *63*(13), 2001–2007. https://doi.org/10.1016/S0016-7037(99)00091-5

Zeebe, R. E., and Zachos, J. C. (2007). Reversed deep-sea carbonate ion basin gradient during Paleocene-Eocene thermal maximum. *Paleoceanography*, *22*(3). https://doi.org/10.1029/2006PA001395

Zweng, M. M., Reagan, J. R., Seidov, D., Boyer, T. P., Locarnini, R. A., Garcia, H. E., et al. (2019). *World Ocean Atlas 2018 Volume 2: Salinity*. (A. V. Mishonov, Ed.). NOAA Atlas NESDIS 82.

Site	Latitude °N	Longitude °E	Region	Depth [m]
A14	8.0	113.4	Pacific Ocean (West tropical)	1911
CD107 A MC	52.9	-16.9	Atlantic Ocean (North)	3569
CD107 B MC	57.4	-42.0	Atlantic Ocean (North)	1100
CD107 C MC	57.1	-31.0	Atlantic Ocean (North)	1925
CD145 A3200	20.0	65.6	Indian Ocean (Central tropical)	3190
CD145 Al50	23.3	66.7	Indian Ocean (Central tropical)	151
CD94 6B (OMEX)	56.6	9.8	Atlantic (North)	1683
E035	26.7	125.3	Pacific Ocean (North western)	326
ELT47-017-PC	-53.4	72.2	Indian Ocean (South)	958
EN066 GGC 10	6.6	-21.9	Atlantic Ocean (Eastern equitorial)	3527
EN066 GGC 16	5.5	-21.1	Atlantic Ocean (Eastern equitorial)	3160
EN066 GGC 21	4.2	-20.6	Atlantic Ocean (Eastern equitorial)	3792
EN066 GGC 38	4.9	-20.5	Atlantic Ocean (Eastern equitorial)	2937
EN066 GGC 51	5.4	-22.7	Atlantic Ocean (Eastern equitorial)	4263
KNR 166-2-26JPC	24.3	-83.3	Gulf of Mexico	546
KNR166-2-110MC	24.5	-79.2	Atlantic Ocean (Southwest sub tropical)	390
KNR166-2-11MC	24.2	-83.3	Gulf of Mexico	750
KNR166-2-28MC	24.2	-83.3	Gulf of Mexico	648
ML1208-13BB	0	-156	Pacific Ocean (Central tropical)	3050
ML1208-36BB	7	-161	Pacific Ocean (Central tropical)	2855
MW91-9 GGC 15	0.0	158.9	Pacific Ocean (Western equitorial)	2311
MW97 MC-28G	0.0	162.2	Pacific Ocean (Western equitorial)	4325
MW97 MC-45A	0.0	161.0	Pacific Ocean (Western equitorial)	3368
OCE 205-2 BC 51	26.2	-77.7	Atlantic Ocean (Western tropical)	830
OCE 205-2 BC 53	26.2	-77.7	Atlantic Ocean (Western tropical)	1038
OCE 205-2 BC 55	26.2	-77.7	Atlantic Ocean (Western tropical)	1140
OCE 205-2 GGC 43	26.3	-77.7	Atlantic Ocean (Western tropical)	479
MW0691 1BC7	-2.2	157.0	Pacific Ocean (West tropical)	1614
MW0691 1BC3	-2.18	157	Pacific Ocean (West tropical)	1616
MW0691 1.5BC11	-1.0	157.8	Pacific Ocean (West tropical)	2016
MW0691 1.5BC33	-1.0	157.8	Pacific Ocean (West tropical)	2015
MW0691 2.5BC37	0	159	Pacific Ocean (West tropical)	2445
MW0691 3BC16	0	160.4	Pacific Ocean (West tropical)	2959
MW0691 3BC24	0	160.45	Pacific Ocean (West tropical)	2965

MW0691 4.5BC53	0	161.4	Pacific Ocean (West tropical)	3711
MW0691 4BC51	0.0	161	Pacific Ocean (West tropical)	3411
MW0691 5BC54	0	161.4	Pacific Ocean (West tropical)	4025
MW0691 5.5BC58	0	162.22	Pacific Ocean (West tropical)	4341
MW0691 6BC74	0	162.7	Pacific Ocean (West tropical)	4438
VM18-222	-38.6	140.6	Indian Ocean (Southeast)	1904
VM20-133	33	140	Pacific Ocean (North western)	1503
VM21-1	38.7	-72.7	Atlantic Ocean (North)	2186
VM28-230	-5	167	Pacific Ocean (West tropical)	2992
VM34-157	-41	26	Atlantic Ocean (Southeast)	3636
WIND 10B	-29.1	47.5	Indian Ocean	3520
WIND 33B	-11.2	58.8	Indian Ocean	2871
WP7_01	-3.9	156.0	Pacific Ocean (West tropical)	1800

Species
Globorotalia menardii, Trilobatus sacculifer
Globoconella inflata, Neogloboquadrina pachyderma, Orbulina universa
Globigerina bulloides
Globigerina bulloides
Globorotalia menardii, Mixed benthic species
Neogloboquadrina dutertrei, Orbulina universa, Trilobatus sacculifer, Cassidulina species, Uvigerina species, Mixed benthic species
Globigerina bulloides
Pulleniatina obliquiloculata
Globigerina bulloides, Neogloboquadrina pachyderma
Cibicidoides species, Hoeglundina elegans, Mixed benthic species
Cibicidoides species, Hoeglundina elegans, Mixed benthic species
Cibicidoides species, Hoeglundina elegans
Cibicidoides species, Mixed benthic species
Cibicidoides species, Hoeglundina elegans
Globigerinoides ruber, Trilobatus sacculifer
Cibicidoides species, Hoeglundina elegans, Planulina ariminensis, Uvigerina species
Cibicidoides species, Hoeglundina elegans, Uvigerina species
Cibicidoides species, Hoeglundina elegans, Uvigerina species
Globigerinoides ruber, Trilobatus sacculifer
Globigerinoides ruber, Trilobatus sacculifer
Mixed benthic species
Mixed benthic species
Mixed benthic species
Cibicidoides species, Mixed benthic species
Hoeglundina elegans, Mixed benthic species
Hoeglundina elegans, Mixed benthic species
Cibicidoides species, Mixed benthic species
Globerginella siphonifera, Globorotalia tumida, Neogloboquadrina dutertrei, Pulleniatina obliquiloculata, Trilobatus sacculifer, Mixed benthic species
Globerginella siphonifera, Pulleniatina obliquiloculata, Trilobatus sacculifer
Neogloboquadrina dutertrei, Pullentina obliquiloculata, Trilobatus sacculifer
Globerginella siphonifera, Globorotalia tumida, Pulleniatina obliquiloculata, Trilobatus sacculifer
Globorotalia tumida, Pulleniatina obliquiloculata, Trilobatus sacculifer, Mixed benthic species
Globorotalia tumida, Pulleniatina obliquiloculata
Globorotalia tumida, Neogloboquadrina dutertrei, Pulleniatina obliquiloculata, Trilobatus sacculifer

Globerginella siphonifera, Globorotalia tumida, Pulleniatina obliquiloculata
Pulleniatina obliquiloculata, Mixed benthic species
Pulleniatina obliquiloculata
Globorotalia tumida, Pulleniatina obliquiloculata
Globorotalia tumida, Pulleniatina obliquiloculata
Globoconella inflata
Neogloboquadrina dutertrei
Globigerina bulloides, Neogloboquadrina dutertrei
Globigerinoides ruber, Trilobatus sacculifer
Trilobatus sacculifer
Trilobatus sacculifer, Cibicidoides species
Trilobatus sacculifer
Globorotalia menardii, Globorotalia tumida, Neogloboquadrina dutertrei, Pulleniatina obliquiloculata, Trilobatus sacculifer